



**3,3'-thiodipropanol as a mounting medium
for high resolution microscopy: a
comparative analysis with similar thiols.**



MAESTRÍA EN CIENCIAS (ÓPTICA)

Asesor

Dra. Valeria Piazza

Presenta

Lic. Milvia Iris Alata Tejedo

*Noviembre de 2017
León, Guanajuato,
México*

Dedication

To Daniel and Blue.

3,3'-thiodipropanol as a mounting medium for high
resolution microscopy: a comparative analysis with
similar thiols.

by

Lic. Milvia Iris Alata Tejedo

DISSERTATION

Presented to the Evaluation Committee of
Centro de Investigaciones en Óptica A.C.

In Partial Fulfillment
of the Requirements
for the Degree of

MAESTRO EN CIENCIAS ÓPTICA

CENTRO DE INVESTIGACIONES EN ÓPTICA A.C.

2017

Acknowledgments

I would like to express my sincere gratitude to my advisor Dr. Valeria Piazza for the continuous support, her motivation and patience. Working with her has been a productive and stimulating experience.

Besides my advisor, I would like to thank the rest of my committee: Dr. Julio César Armas Pérez and Dr. Mario Alejandro Rodríguez Rivera, for their insightful comments.

I would like to thank all the teachers and friends that shared this process with me and made it an amazing experience.

I gratefully acknowledge the funding sources that made my work possible. I thank Consejo Nacional de Ciencia y Tecnología (CONACyT-México) for the scholarship received during my master studies. The work I present here is part of a project called "Desarrollo de nuevos medios de montaje para microscopia con alta resolución", convenio SICES number 094/2016CIO, funded by Consejo de Ciencia y Tecnología del Estado de Guanajuato (CONCYTEG). I thankfully acknowledge the computer resources, technical expertise and support provided by the Laboratorio Nacional de Supercómputo del Sureste de México, CONACYT network of national laboratories."

Last but not least, I would like to thank my family: my husband and daughter for supporting me throughout writing this thesis and my life in general.

Abstract

The purpose of this work is to analyze the optical, chemical and biological behavior of four chemicals similar to 2,2'-thiodiethanol (TDE), in the perspective of their use as mounting media for high-resolution fluorescence microscopy. TDE, the model molecule in this work, was shown to possess many properties that make it an excellent fluid for the preparation of microscopy slides. Its drawback is the lack of compatibility with the most popular reagent for actin staining, the toxin phalloidin. Due to the relevance of phalloidin in terms of quality of actin decoration, simplicity of protocol and popularity, our aim is to find a compound similar to TDE, in terms of optical properties and structure that would allow the phalloidin-conjugated fluorophores to be used.

Three molecules with structural affinity to TDE were proposed as mounting media for fluorescent microscopy: Butyl sulfone (BTS), 3,3'-thiodipropanol (TDP), 2,2'-sulfonyldiethanol (SDE). In this work, the molecules were tested for solubility in water and their refractive indices were measured at different concentrations in water, finding a linear relation between the refractive index and the concentration. Absorption and fluorescence spectra of four different fluorophores in PBS, and in the analyzed mounting media – TDE and TDP - have been obtained. Cells stained with conjugated phalloidin were mounted using the previously mentioned media and imaged in a confocal fluorescence microscope. Fluorescence of conjugated phalloidin was not observed when cells were mounted in SDE. Labeled cells mounted in TDP showed fluorescent labeling and preserved their f-actin structures.

In parallel, additional experiments and molecular simulations were done for trying to elucidate the mechanism that hinders the phalloidin staining of actin in the

presence of TDE. As a first attempt a phalloidin system was solvated with TDE, finding that there was no interaction between them, suggesting that the mechanism might be related to interaction between F-actin and TDE.

Experiments indicate that the probe bonded to F-actin diffuses in TDE. Two reasons could explain the diffusion, depolymerization of F-actin caused by TDE, or occupation of f-actin binding site by TDE.

Resumen

El propósito de este trabajo es analizar el comportamiento óptico, químico y biológico de cuatro químicos similares a 2,2'-thiodiethanol (TDE), con miras a su uso como medio de montaje para microscopía de fluorescencia de alta resolución. Recientemente se demostró que la molécula TDE, que ha sido tomada como modelo para este trabajo, posee propiedades que la hacen un excelente fluido para la preparación de laminillas para microscopia. Su desventaja es la incompatibilidad que presenta con el reactivo más popular para el marcaje de actina, la toxina faloidina. Debido a la relevancia de faloidina en términos de calidad para el marcaje de actina, simpleza del protocolo y popularidad, nuestro objetivo es encontrar un compuesto similar a TDE que permita el uso de fluoróforos conjugados a faloidina.

Tres moléculas con afinidad estructural a TDE fueron propuestas como medio de montaje para microscopía de fluorescencia: Butil sulfona (BTS), 3,3'-tiodipropanol (TDP) and 2,2'-sulfonildietanol (SDE). En este trabajo, se probó la solubilidad de las moléculas en agua, encontrando una relación lineal entre el índice de refracción y la concentración. Los espectros de absorción y emisión de cuatro fluoróforos en PBS y en los medios de montaje analizados – TDE, TDP - han sido obtenidos. Las células teñidas con faloidinas conjugadas fueron montadas usando los medios mencionados previamente y luego se tomaron micrografías de fluorescencia en un microscopio confocal. No se observó fluorescencia de faloidinas conjugadas cuando las células estaban montadas en SDE. Las células teñidas y montadas en TDP mostraron marcaje fluorescente y preservaron las estructuras de los filamentos de actina.

En paralelo, experimentos adicionales y simulaciones moleculares se realizaron para tratar de elucidar el mecanismo que obstaculiza el marcaje de los filamentos de actina

con faloidinas en la presencia de TDE. Como primera aproximación de las simulaciones, un sistema de faloidinas fue solvatado con TDE, encontrando que no hay interacción entre TDE y las faloidinas. Este resultado sugiere que el mecanismo debe estar relacionado con la interacción entre los filamentos de actina y TDE.

Los experimentos indican que la sonda unida a los filamentos de actina se desplaza en presencia de TDE. Dos razones pueden explicar este desplazamiento, depolimeración de los filamentos de actina u, ocupación del sitio en que faloidina debe unirse a los filamentos por TDE.

ACKNOWLEDGMENTS.....	IV
ABSTRACT	V
RESUMEN	VII
INTRODUCTION.....	1
1.1 Refractive index mismatch.....	1
1.1.1 Difference between actual and apparent size of an object in z axis.....	3
1.1.2 Reduction of the effective numerical aperture.....	4
1.1.3 Reduction in resolution and peak intensity	6
1.2 Optical microscopy	7
1.2.1 Resolution and Point spread function.....	8
1.2.2 Contrast.....	9
1.2.3 Phase contrast microscopy.....	10
1.2.4 Confocal fluorescence microscopy	11
1.3 Cell preparation for fluorescence microscopy	14
1.3.1 Cells and microscopy	14
1.3.2 Cell culture.....	15
1.3.3 Preparation of the cell slide for fluorescence microscopy.....	17
1.3.3.1 Fixation.....	17
1.3.3.2 Staining of samples.....	18
1.3.3.2.1 Chemical dyes.....	19
1.3.3.2.2 Fluorescent proteins	20
1.3.3.2.3 Antibodies	20
1.3.3.3 Samples mounting.....	21
1.3.3.3.1 Mounting.....	21
1.3.3.3.2 Candidates for mounting medium based on TDE.....	23
1.3.4 Actin cytoskeleton, our structure of interest	27
1.3.5 Staining the actin cytoskeleton.....	28
1.4 Molecular dynamics simulation	30
1.4.1 Molecular interactions.....	30
1.4.2 GROMACS.....	31
1.4.2.1 Units used in GROMACS	31
1.4.2.2 Reduced units.....	32
1.4.2.3 Periodic boundary conditions.....	32
1.4.2.4 Cut-off restrictions	33
1.4.3 The global MD algorithm	33

1.4.5 Force field	35
1.4.6 Potential energy.....	36
MATERIALS AND METHODS	38
2.1 Mounting Media	38
2.2 pH adjustment.....	39
2.3 Refractive index measurement.....	40
2.4 Fluorescence dyes	44
2.5 Spectra measurements.....	44
2.6 Cell culture and immunocytochemistry	46
2.6.1 Culture method.....	46
2.6.2 Fixation Method.....	47
2.6.3 Staining method.....	48
2.6.4 Mounting.....	49
2.7 TDE effect on F-actin labeled with fluorescent phalloidins.	50
2.8 Imaging	51
RESULTS.....	53
3.1 Refractive index of candidates for mounting media	53
3.2 Dispersion measurements	55
3.3 Absorption and emission spectra.....	58
3.4 Standard staining using fluorescent phalloidins.....	61
3.5 Micrographs obtained using candidates	65
3.5.1 Cytoskeleton of cells mounted in TDP	66
3.5.2 Microtubules of cells mounted in TDP	70
3.6 Understanding loss of fluorescence of the actin filaments in presence of TDE	71
3.7 Molecular dynamics	78
CONCLUSION AND FURTHER WORK.....	84

REFERENCES.....	86
APENDIX 1	90
APENDIX 2	91

Introduction

1.1 Refractive index mismatch

In the case of imaging biological samples mounted in microscopy slides, the optical system includes the space between the lens and the sample, and the sample itself. It has to be considered that biological samples often need to be mounted on a surface (slide) and covered (coverslip) to be imaged. This process increases the number of surfaces light must cross before reaching the sample and adds a new challenge: optimizing the optical properties of sample to be imaged in order to get a better resolution.

On one side lenses in microscopes have evolved to the immersion lenses and high numerical apertures due to their capability of reducing spherical aberration and improving resolution and intensity of the signal. It was Hooke, the same one that first looked at a cell, who first addressed this subject. He wrote in 1678 in *Microscopium*: "*that if you would have a microscope with one single refraction, and consequently capable of the greatest clearness and brightness, spread a little of the fluid to be examined on a glass plate, bring this under one of the globules, and then move it gently upward till the fluid touches and adheres to the globule*" [1]. But it was not until 1840 that Amici made the first immersion objectives [2]. Although he designed them to be used with oil, scientist were not willing to put oil onto expensive slides, so the liquid of choice became water and therefore many designs were developed using water as immersion liquid. About 30 years later, Zeiss produced oil immersion objectives designed by Abbe. The refractive index of glass coverslip and immersion oil is 1.518.

With the development of oil immersion lenses the light path is refractive index homogeneous until it reaches the specimen. As is shown in Figure 1.1 light must cross oil immersion and glass of the same n , then it finds the sample immersed in a mounting medium. This mounting medium is a material that is used to preserve the features of the biological specimen and is also a material that will interact with light, that is the reason why its refractive index is an important characteristic.

Some of the possible consequences of changes of n at the glass-mounting medium boundary: refraction of light inducing rays to focus at different positions in z axis than they would if the system were perfectly matched and generating a difference between the actual size of an object in z axis and its apparent size, reduction of the effective numerical aperture (NA) and, as waves are deviated from their sphericity, reduction in resolution and peak intensity [3].

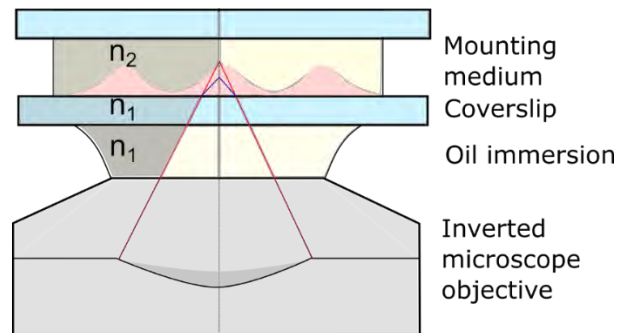


Figure 1.1 Inverted microscope objective illuminating a sample. Red lines describe light path when the system is homogeneous ($n_1 = n_2$), the blue lines inside the sample show the refraction of light when the refractive index of the mounting medium is lower than the refractive index of the coverslip.

1.1.1 Difference between actual and apparent size of an object in z axis

The distances measured along the optical axis are smaller than the geometrical distances in the object [4], [5], [6]. To illustrate this situation, consider a light cone of converging light that travels through a medium with refractive index n_1 focusing in a second medium with refractive index n_2 . Marginal rays from the light cone form an angle of incidence θ_1 with the normal to the interface, and an angle θ_2 , a refraction angle, as seen in Figure 1.2. This figure shows the geometry of marginal rays incident to a point P in a sample after refraction when $n_1 > n_2$

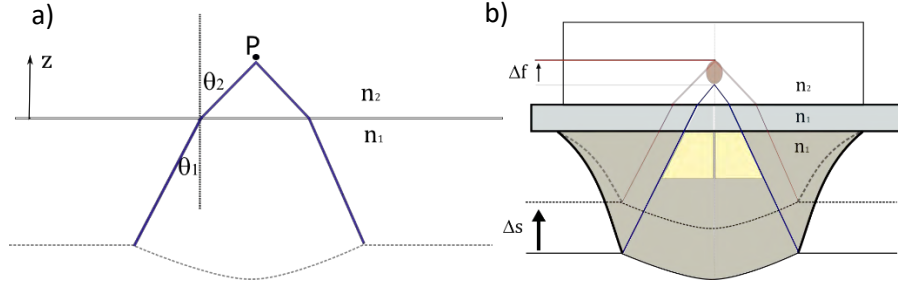


Figure 1.2 Refraction of a light beam at the coverslip-mounting medium interface for $n_1 > n_2$. a) Geometry of refraction at the glass-mounting medium interface, where θ_1 is the angle of incidence and θ_2 is the refraction angle. b) Difference between the displacement of the objective Δs and the displacement of the focal spot Δf .

If the specimen is moved towards the lens to a distance Δs in the z direction, the focal plane is displaced a distance Δf Eq. (1.1) [5].

$$\Delta f = \frac{\tan \theta_1}{\tan \theta_2} \Delta s \quad (1.1)$$

Which written in terms of the numerical aperture $NA = n_1 \sin \theta_1$ gives:

$$\Delta f = \frac{\tan \left[\sin^{-1} \left(\frac{NA}{n_1} \right) \right]}{\tan \left[\sin^{-1} \left(\frac{NA}{n_2} \right) \right]} \Delta s \quad (1.2)$$

With this simple approach we can predict $\frac{\Delta s}{\Delta f}$

Objective Lens: 63X Oil immersion

NA = 1.4, $n_1=1.518$, $\theta_1 = 67^\circ$

Mounting Medium	n_2	$\frac{\Delta s}{\Delta f}$
Water	1.33	NA reduced, critic angle 61° .
75% Glycerol	1.44	1.74
Vecta shield	1.457	1.45
ProLong diamond	1.47	1.3
3,3'-thiodipropanol	1.5	1.09
2,2'-thiodiethanol	1.518	1

Table 1.1 The value $\frac{\Delta s}{\Delta f}$ indicates how many times the size of object is increased due to n mismatch.

Table 1.1 shows $\frac{\Delta s}{\Delta f}$ in case of imaging biological samples with an oil immersion objective of $NA = 1.4$ and $\theta_1 = 67^\circ$, using different mounting media. The calculations made according to Eq. (1.2) indicate that the apparent depth of the object is 1.74 times the actual depth when 75% glycerol is the mounting medium. This effect is reduced as n_2 approaches n_1 . Following these calculations the conclusion is that, if $n_1 > n_2$, objects will look bigger that they are, but if $n_2 > n_1$, they would look smaller in the z direction.

1.1.2 Reduction of the effective numerical aperture

The reduction of the effective NA occurs because of total internal reflection [3]. When light reaches the interface between the glass and the mounting medium refraction and also reflection occur. If we know the incidence angle, and the refractive indices of both media we can calculate refraction angle by Snell's law Eq. (1.3).

$$n_1 \sin \theta_1 = n_2 \sin \theta_2 \tag{1.3}$$

The refraction angle is $\theta_2 = \sin^{-1}\left(\frac{n_1 \sin \theta_1}{n_2}\right)$; this result introduces a critical angle, the biggest incident angle for which there is still refraction and besides that critical angle there is total internal reflection.

For the case of water as mounting medium in table 1., $n_1 = 1.518$, $n_2 = 1.333$ and $\theta_1 = 67^\circ$: for this angle of incidence $\sin \theta_2 = 1.05$. But $\sin \theta$ is a function defined between -1 and 1; 1.05 is out of the range so the angle 67° is beyond the critical angle and there is no refraction. The critical angle in this case is 61° , given by the same refractive indices and assuming $\sin \theta_1 = 1$. In this case the NA has been reduced to 1.3.

Figure 1.3 illustrates the effective reduction of NA and means that not all rays from the cone of light will be refracted only the ones with an incident angle lower than the critical one.

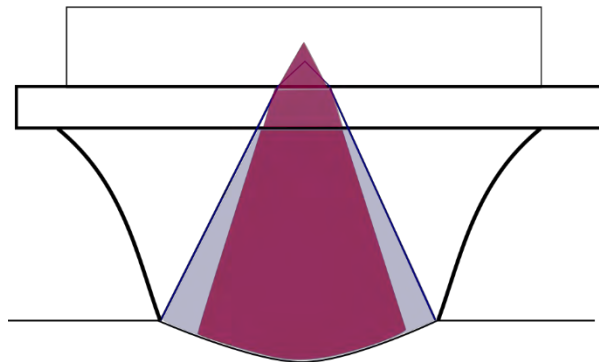


Figure 1.3 The blue cone represents light gathered by a high NA objective when the system is homogeneous, and the red zone is the light gathered through the reduced effective NA when the refractive index of the mounting medium is lower.

1.1.3 Reduction in resolution and peak intensity

In optical microscopy, resolution refers to the minimal distance between two points in the sample that a system is able to differentiate. Image resolution is determined by diffraction of light caused by the specimen, and the objective [3].

In the xy plane, resolution is described by the Eq. (1.4) which is a function of the objective lens's NA and the wavelength of the excitation light according to Ernst Abbe's diffraction limit expression:

$$r_{lateral} = 0.61 \frac{\lambda_0}{NA_{obj}} \quad (1.4)$$

where r is expressed as the distance in the specimen plane, λ_0 is the wavelength of light in vacuum; and NA_{obj} is the numerical aperture of the objective lens. NA is the product of the sine of the half angle θ_1 of the cone of light collected by the objective lens and the refractive index of the imbibing medium between the specimen and the objective lens.

Axial resolution, measured along the optical axis of the microscope is described by Equation 1.5.

$$r_{axial} = \frac{2\lambda_0 n}{NA_{obj}^2} \quad (1.5)$$

Both Equations 1.4 and 1.5 depend on NA_{obj} , and so on the half aperture angle θ_1 and n , showing that the election of the mounting medium is going to affect the resolution of the optical system. However, r_{axial} is inversely proportional to the square of the NA_{obj} , making axial resolution more susceptible to changes in refractive index [7]. The refractive index mismatch increases spherical aberrations and these reduce spatial resolution [8].

Signal intensity is affected by refractive index mismatch because it also depends on NA. In Equation 1.6 collected light flux is described in terms of the size of emitting surface element dA and the square of the NA , if a flat specimen is imaged [9].

$$\Phi_{n,dA} \propto dA\pi NA^2 \quad (1.6)$$

Where $\Phi_{n,dA}$ is the light flux and dA is the surface differential. Finally, light collection is proportional to NA^2 and impacts directly into image brightness.

1.2 Optical microscopy

Optical microscopy refers to the use of light and the magnification of a lens to observe a sample. Hooke and Leeuwenhoek are known to be the first to publish work based upon the use of an optical microscope in the middle of the 17th century.

By the 19th century, compound microscopes capable of high magnification and good resolution were already available. This was possible because of the improvements in lenses design and the comprehension of spherical and chromatic aberrations leading to the design of optical systems that are able to reduce them, improving the resolving power of optical microscopes. But there was a limit on optical resolution: according to Ernst Abbe and Lord Rayleigh [10], [11], light of wavelength λ focused by a lens of numerical aperture, $NA = n \sin \alpha < 1$ will not allow the differentiation of two points closer together than a distance $d = \frac{\lambda}{2NA}$, because diffraction will merge their images. According to this equation, the higher the numerical aperture and the shorter the wavelength, the better the resolving power.

1.2.1 Resolution and Point spread function

Huygens postulated that light at its most elemental part is a perturbation that propagates in all directions as a spherical wave. He called these elements of light wavelets. They are the elemental unit of waves whether waves are plane or spherical. In the case of plane waves, they are aligned over a line and, for spherical waves, they are in the surface of a sphere that can be either converging or diverging. When multiple wavelets from the same source and at the same time (i.e., coherent) interact, they set up standing waves of constructive and destructive interference.

The final goal of microscopy is to focus light in a focal spot and assure constructive interference of the wave front focusing in this point. Constructive interference generates a spot around the focal point, which is mathematically described by the point spread function (PSF). When the PSF is smaller the image has better resolution, the improvement is achieved by increasing the aperture angle allowing more wavelets to interfere and generate a smaller PSF. But lenses focus only a segment of the spherical wave that originates from just one side of the focal plane, producing a spot that is larger than wider, leading to a difference between axial and lateral resolution [12]. This situation is described in Figure 1.4

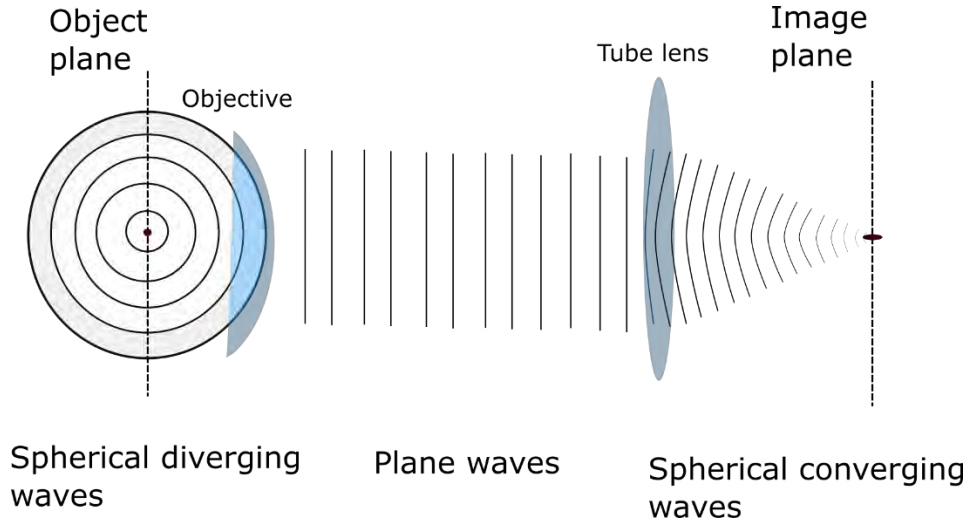


Figure 1.4 Schematic representation of the focusing process. A spherical diverging wave goes through the objective lens and a plane wave comes from it, the plane wave goes through the tube lens and focuses on a point on the image plane. Because the process is unidirectional the focal spot is longer than wider.

1.2.2 Contrast

Apart from resolution, another important aspect in microscopy is contrast, which is defined as the difference of intensity between the image and the background. Differences in intensity and color are the ones that generate contrast and allow sample visualization. For the human eye, the minimal contrast difference to distinguish between image and background is 2%.

In general, contrast is measured by the relationship between the highest and lowest intensity in an image, and can be described by:

$$\text{Percent Contrast} = [(I_b - I_s)/I_b] \times 100 \quad (1.7)$$

where I_b is the background intensity and I_s is the intensity of specimen features for which contrast is being investigated.

Most biological samples lack of intrinsic contrast, thus to be imaged optical techniques to generate contrast must be used like phase contrast microscopy or introduction of dyes into cells or tissue. In case of fluorescence microscopy, specimens that not fluoresce, need to be labeled using probes that might recognize a particular biological target and bind to it without inducing significant perturbations [3].

In this project, a phase contrast microscope has been used for monitoring cell cultures, and a confocal fluorescence microscope to image stained cells

1.2.3 Phase contrast microscopy

The Dutch physicist Fritz Zernike developed a technique that converts a phase object, essentially transparent like cells or bacteria, into an amplitude object, with an observable intensity, making it visible to our eyes under a microscope. The difference between changes induced in light by a phase object and an amplitude object is shown in Figure 1.5.[13]

While working with diffraction gratings Zernike understood how interference affects image formation. He applied this idea to a microscope, by introducing a phase shift only in illumination light to change the way it interferes with light diffracted by a phase object [14]. The diffraction pattern of the transparent object is now similar to that of an absorbing specimen and the interference of illumination light and diffracted light results in a visible image.

As shown in Figure 1.6, the specimen is illuminated by the light coming from a ring (condenser annulus). The diffracted and undiffracted light is separated in space by allowing the selective manipulation of their phases and intensities.

This technique had big impact in biology because it allowed the examination of living specimens without introducing any modification like staining or fixation, and also the possibility of observing time-dependent processes like cell motility, apoptosis and cell division.

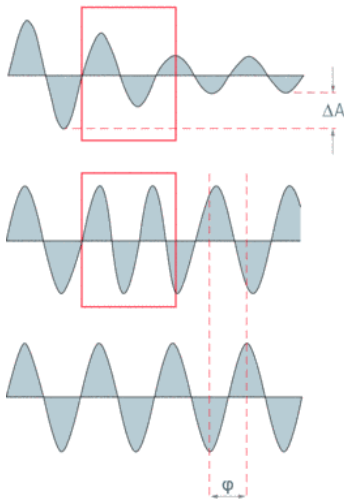


Figure 1.5 The red boxes represents objects, in the upper row an amplitude object and in the second row a phase object. When light goes through an amplitude object, light amplitude is reduced (ΔA) and is detected as a loss of brightness. When light goes through a phase object its phase changes (φ) but the human eye can not identify it. At the last row we have an unchanged wave.

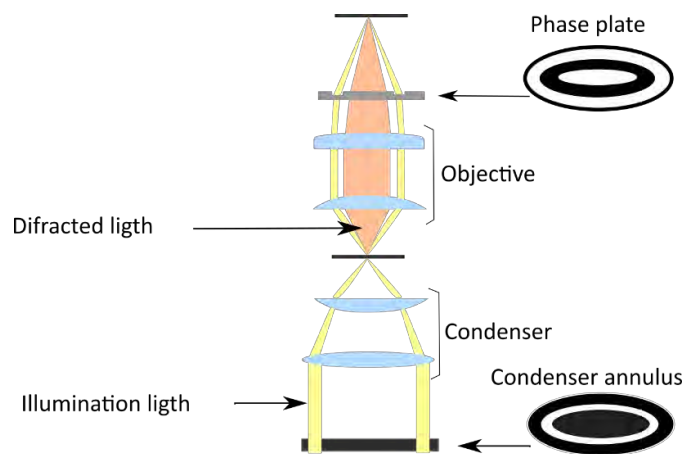


Figure 1.6 Optical diagram of a phase contrast microscope.

1.2.4 Confocal fluorescence microscopy

Wide field fluorescence microscopy and confocal microscopy are both techniques used to investigate fluorescent samples. On wide field fluorescence microscopy, the whole field of view is evenly illuminated. The fluorescent sample is excited causing all the

specimen thickness to fluoresce. The out of focus light cannot be separated from the in focus detail, reducing image contrast. In confocal microscopy a laser light source is focused in the sample, reducing the illuminated volume. Only the focal volume could fluoresce and the emitted light is collected by an objective and passes through a pinhole positioned confocal to the focal spot.

The consequence of this restricted light path is that only light coming from the thin focal section contributes to the image. This technique allows to take images of different focal planes which can be recombined to create a three dimensional representation of the sample.

The confocal laser scanning microscope (CLSM) was developed by Marvin Minsky in 1957 [3]. He proposed to replace the conventional condenser by a microscope objective and restrict the illumination by a pinhole at the microscope axis, he also restricted the field of view with another pinhole in the image plane positioned confocally to the illumination spot in the specimen and to the first pinhole as is shown in Figure 1.7.

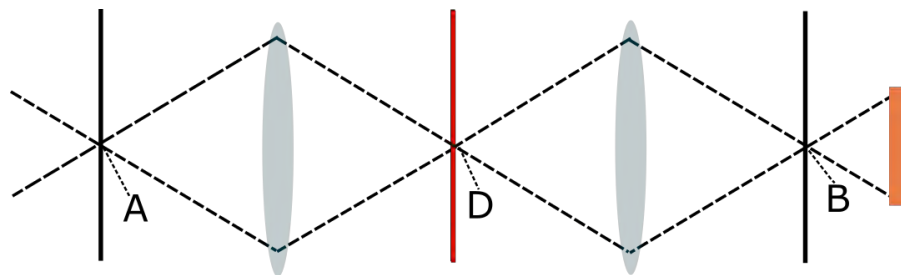


Figure 1.7 shows a schematic illustration of the layout of a confocal scanning microscope. The pinholes are in A and B, D is the confocal spot in the specimen. The lenses are shown in blue and the detector in orange, the dashed lines indicate the light path.

The idea behind this design is to reject light scattered from parts other than the illuminated point on the sample, from the optical system, and is called optical

sectioning. This is why confocal laser scanning microscopy is a technique that increases the contrast of the image by restricting the imaged volume, improving image resolution compared to conventional microscopy [15].

The confocal microscope can also be set up in an epi-illuminating mode, instead of trans-illuminating the sample, by using the same objective as condenser and objective lens. To image a specimen the light has to illuminate it point by point in a raster pattern; this is achieved by using angle adjustable mirrors.

Among the advantages provided by CLSM are the possibility of using it with multiple dyes in the sample, the possibility to achieve high resolution without any post processing, 3-d reconstruction and good compatibility with live cell imaging.

	Wide field + deconvolution	Confocal laser scanning	Super-resolution techniques
Acronym	N.A.	CLSM	Moiré effect (SSIM), STED, PALM/STORM
XY- resolution	180-250 nm	180-250 nm	50 nm, 20- 100 nm, 20-50 nm
Z- resolution	500-700 nm	500-700 nm	N.D, 560 nm, 100 nm
Z stack range	100 um	100 um	N.A., > 20um, few microns
Dyes	Any	Any	Special dyes
Simultaneous colors	>3	>3	1, 2, 2
Live cell imaging	Yes	Yes	No, restricted, restricted
Post processing required	Yes	No	Yes

N.A. not applicable, N.D. not described.

Table 1.2 Fluorescence microscopy methods. Adapted from [15].

At present, techniques that achieve resolution beyond the diffraction barrier, proposed by Abbe, are already available. Super-resolution light microscopy methods include saturated structured illumination microscopy (SSIM), stimulated emission depletion microscopy (STED), photo-activation localization microscopy (PALM), and stochastic optical reconstruction microscopy (STORM), among others. A

comparison between fluorescence-based techniques like wide field, confocal laser scanning and super-resolution microscopy is shown in Table 1.2.

1.3 Cell preparation for fluorescence microscopy

Fluorescence microscopy is the most popular technique in biological imaging because of its high sensitivity and specificity, allowing the use of various different fluorophores at the same time [16].

This section summarizes relevant processes involved in cell preparation for fluorescence microscopy and concepts related to the cell lines used in this work.

1.3.1 Cells and microscopy

Cell is the unit of life. All living organisms are composed by at least one cell, but it wasn't until 1665 when Robert Hooke observed through his microscope a thin slice of cork that their existence was proved. In 1838 Schwann and Schleiden formulated the first cell theory thanks to the power offered by achromatic lenses developed eight years before, yet at that time the cell seemed to be just a membrane and a nucleus. In 1877, the development of oil immersion lenses, and advances in sample preparation and dyes allowed scientist to observe into cells and differentiate structures [17].

Optics and biological improvements, together, were necessary to develop techniques that allowed the observation of subcellular structures. In the second half of 20th century, cell biology made unprecedented progress: the first continuous cell line was subcultured [18], the nutritional needs of animal cells in culture were defined [19], transfection methods were developed and green fluorescent protein in jellyfish was discovered and then isolated [20], among others.

1.3.2 Cell culture

Cell culture is the process by which cells that have been isolated from their original tissue by enzymatic or mechanical means could be maintained in an artificial environment. Such cells require special conditions to survive, including being maintained in a solution with nutrients and growth factors, at an ideal temperature, humidity, gaseous atmosphere and appropriate substrate.

In this favorable conditions cells proliferate, and in case of adherent cells they occupy all the substrate they are growing in. At this point they need to be subcultured, which means transferred them to a new vessel with fresh growth medium and enough space to continue growing [21].

Cell lines can be finite or continuous. Continuous cell lines are also known as immortalized because through genetic mutations or artificial modifications they have acquired the ability to proliferate indefinitely. On the other hand, finite cell lines can only be subcultured for 20-80 passages after that they senesce.

Cells in culture can be divided in three categories according to their morphology: fibroblastic, epithelial-like and lymphoblast-like. Fibroblastic-like cells are polar or multipolar, elongated and grow attached to substrate. Epithelial-like cells are polygonal and grow attached to a substrate in discrete patches. Lymphoblast-like cells are spherical in shape and usually grown in suspension without attaching to a surface.

Three cell lines have been used in this work: Hek 293, HeLa and Sh-sy5y. The first two are continuous cell lines, their morphology is epithelial-like, polygonal shaped

and grow as adherent cells. The third is also epithelial but includes both adherent and floating cells, and can be subcultured for a limited number of times.

HEK293 is a cell line originally derived from human embryonic kidney cells. They were transformed by exposing them to fragments of adenovirus type 5 DNA by Frank Graham in 1977 [22]. This cell line is of common use because of its reliable growth and propensity for transfection.

HeLa cells are the first human cancer cell line immortalized in tissue culture, extracted from a cervix cancer patient, Henrietta Lacks. This cell line was cultured by George Otto Gey in 1951 [18], and found to be remarkably durable.

SH-SY5Y is a cloned subline of the neuroblastoma cell line SK-N-SH originally isolated from a metastatic bone tumor biopsy by June L. Biedler and Barbara A. Spengler in 1970 [23]. Bone marrow was taken from a 4-year-old female child suffering from neuroblastoma.

Their morphological characteristics allowed us to image different cytoskeletal structures, in case of HeLa stress fibers are the predominant structures, in case of Hek 293 lamellopodia and in case of SH-SY5Y lamellopodia.

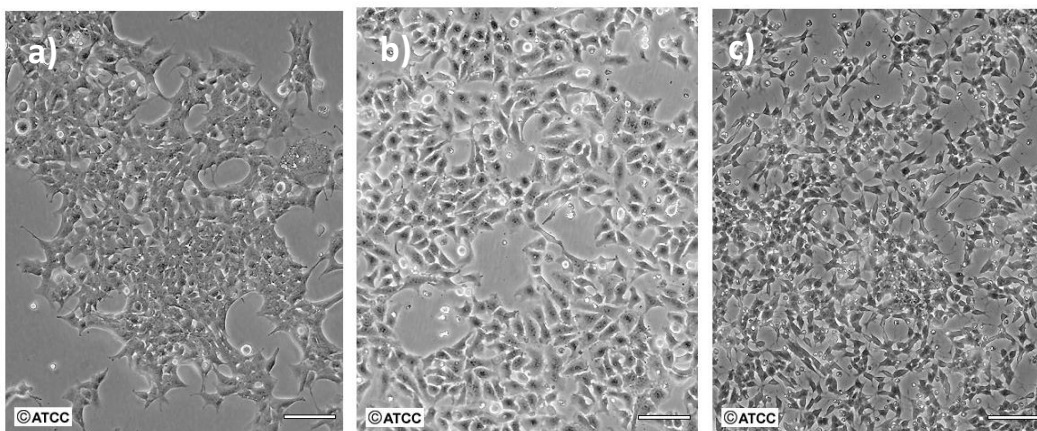


Figure 1.8 Phase contrast images of the three cell lines used in this project a) Hek293, b) HeLa and c) Shsy-5y. Scale bar is $100 \mu\text{m}$ [24].

1.3.3 Preparation of the cell slide for fluorescence microscopy

1.3.3.1 Fixation

To image cell structures that are not changing in time it is necessary to stop cell's metabolism and at the same time preserve the structures of interest. The process by which all biochemical and proteolytic processes are inactivated and structures are immobilized is called fixation.

There are three types of fixation available for biological specimen preparation. Chemical fixatives fix tissues either by coagulating proteins or by chemically crosslinking them. The other two methods of fixation are freeze substitution and microwave fixation.

Coagulating fixatives fix the specimen by changing the hydration state of the cellular component. These fixatives tend to preserve the antigen recognition sites for immunolabeling very well. Ethanol, methanol and acetone are coagulating fixatives.

Crosslinking fixatives include glutaraldehyde, formaldehyde and ethylene glycol bis-succinimidyl. They form covalent crosslinks that are determined by the active group in each compound [3].

For the preservation of cellular structures, crosslinking fixatives are usually superior to agents that precipitate and coagulate proteins. Crosslinking agents also permit binding of mushroom *Amanita phalloides* toxin phalloidin to the actin cytoskeleton for very dense labeling of actin [25], [26]. In this work formaldehyde fixation was

chosen because the goal is to improve imaging of F-actin with phalloidin conjugated dyes.

For the fluorophores to have access to intracellular structures, cells need to be permeabilized. Coagulating fixatives like methanol and acetone are also permeabilization reagents and, when used, no additional permeabilization is needed. On the other hand, when choosing crosslinking fixatives, mild detergents as Triton X-100 and Tween-20 have to be used for this purpose [27].

When the staining is performed with the use of antibodies, another step is needed before staining, blocking. Blocking is important for minimizing unspecific binding of the primary antibody within the cell. To achieve this, proteins from Bovine Serum Albumin (BSA), milk powder or serum can be used.

1.3.3.2 Staining of samples

Size and transparency of cells make them invisible, even when observing them through a microscope. Contrast should be created in the system to distinguish features of cells. This contrast can be generated either by optical techniques, like phase contrast microscopy or by introducing dyes into cells.

Chemistry contributed with the development of different dyes and fluorescent molecules used to label cell structures. Dyes are molecules that do not associate with a particular biological target, and probes are dyes capable of detecting specific biological targets like cells in a tissue, organelles, proteins, nucleic acids, ions and enzymes [3].

The methods for delivering fluorescent compound in specific locations in the cells can be divided into three groups: fluorescent proteins, fluorescently labeled antibodies and chemical dyes with an affinity for particular subcellular component.

Usually more than just one structure is observed, using in the same sample more than one of the methods listed above, increasing the information that can be obtained from the sample; when this is done it is important to assure that the optical properties of the labels do not overlap [28].

1.3.3.2.1 Chemical dyes

The beginning of the nineteenth century represented a fertile period for organic chemistry due to the big demand for textile dyes. Some of these dyes were found to stain biological tissue and even show preference for some parts of the cell. Examples are Eosin, *Malachite green*, *Sudan black*, and *Coomassie blue*. Dyes like these are widely used in histology [29].

One of the most widely used dyes is fluorescein mostly because it is excited by the 488 nm argon-ion laser line. And for multiple color labeling applications coumarins were the choice for blue ~450 nm, and rhodamines for orange ~580 nm. However these dyes showed limitations: fluorescein is pH sensitive, rhodamine aggregates in aqueous solutions and coumarines are comparably less efficient than fluorescein.

New dyes for biomolecular detection applications are always been developed to overcome this type of limitations. The dyes used in this thesis belong to the family of the Alexa Fluor fluorophores, which are more water soluble than fluorescein and rhodamine and exhibit a pH insensitivity over a very broad range (4 – 10) [30].

1.3.3.2.2 Fluorescent proteins

The story of Fluorescent Proteins began with the isolation of green fluorescent protein from *Aequorea victoria* jellyfish by Shimomura. Later this protein has been extensively studied and modified giving birth to a vast number of useful blue, cyan and yellow mutants. Fluorescent proteins from other species have been identified giving more variety to the color palette including orange, red and far red. Fluorescent proteins need to be expressed by the cell so they are used in living cells.

1.3.3.3.3 Antibodies

In 1941 Coon and collaborators first used fluorescent antibodies to localize proteins using the high specificity of immune reactions of the animals [31].

An antibody is a Y- shaped globular protein that reacts specifically with the antigen that induced its formation and is produced mainly by plasma cells. Biotechnology has allowed the production of fluorescent markers by attaching fluorophores to antibodies.

The technique used to label a specific protein or antigen in cells by the use of an antibody, is called immunocitochemistry.

Immunocitochemistry is commonly accomplished either by using fluorophore-conjugated primary antibodies raised against a specific protein (direct immunofluorescence), or by first labeling with primary antibodies followed by secondary antibody detection (indirect immunofluorescence).

Antibodies are produced using an animal species as the host. The most common species for primary antibody are rat, mouse, goat and rabbit, and for secondary goat, donkey, sheep and rabbit.

1.3.3.3 Samples mounting

1.3.3.3.1 Mounting

After completing the immunofluorescence procedure, the samples are usually mounted to facilitate microscope observation. For this purpose a mounting medium is used, which maintains the sample on a microscope slide and prevents its dehydration, as the preservation of sample for imaging is the final goal of the mounting procedure. The choice of mounting medium will depend on different factors like specimen compatibility, toxicity, dye stability, refractive index and cost.

There is a wide variety of commercial mounting media used by biologist and they can be resinous, aqueous, hardening and also mixed with antifade reagents [32]. One important characteristic of a mounting medium is its refractive index because it will affect the sample rendering.

In the search for mounting media with ideal refractive index, resinous materials like Canada Balsam and Dammar balsam ($n=1.52- 1.54$) are used but they are not suitable for fluorescence due to their auto-fluorescence. Most of the media with high refractive indices require dehydration of the sample like the ones named before and BAG or methyl salicylate (listed on table); this step involves time and could be avoided if another mounting medium is used.

Characteristics of the ideal mounting medium

- RI should be as close as possible to that of glass, i.e., 1.52.
- It should be colorless and transparent.
- It should not cause the dye to diffuse or fade.
- It should have no adverse effect on tissue components.

Mounting medium	Refractive index	Cost / mL in U.S Dollars	References
Gel Mount	1.358	\$ 4	[33],[34]
Methyl Salicylate*	1.536	\$ 0.11	[33]
Glycerol	1.477	\$ 3.45	[33]
75% Glycerol	1.44		
Mowiol	1.41-1.49	\$ 4.58	[33]
Vectashield	1.46	\$ 13.5	[35]
Fluoromount	1.40	\$ 3.86	[33]
	1.389		
Fresh Prolong Gold / Diamond	1.39	\$ 23.8 / 25.13	[36]
	After curing 1.44/ 1.47		
DMSO	1.48	\$ 0.7	[38]
97% TDE (2,2'-thiodiethanol)	1.515	\$ 0.31	[37]
BAG* (53% benzyl alcohol, 45% glycerol and 2% N-propyl gallate)	1.513	\$ 2.37	[38]
TDP (3,3'-thiodipropanol)	1.506	\$ 16.6	[33]

Table 1.3 Summary of some of the commercially available mounting media, their prices and refractive indices. * Requires dehydration.

In high resolution microscopy immersion objectives are used. The immersion liquid has a refractive index that matches the refractive index of glass to assure a homogeneous medium between objective and sample. To take full advantage of this immersion optics it is necessary to match the refractive index of the mounting medium to that of the objective's immersion medium whether it is water (n=1.33), glycerol (n=1.47), or oil (n=1.518).

This adds a new characteristic for the mounting medium, the capability of tuning its refractive index from that of water to that of oil immersion.

Among the most used mounting media in fluorescence microscopy are 75% glycerol (n=1.44), Vectashield (n=1.457), Fluoromont G (n=1.4), mowiol (n=1.49), Prolong Gold (n= 1.39- 1.44 hardening) but none of these media are optimal for either water or oil immersion objectives [39], [40],[41]

2,2'-thiodiethanol (TDE) is a water soluble, non-toxic embedding medium of recent characterization which refractive index can be tuned from 1.33 to 1.52 allowing the exact adjustment to that of oil immersion (1.518) when it is prepared using 97% TDE and 3% PBS. TDE is a viscous, clear yellow or transparent liquid used as a solvent. It is the hydrolysis product of sulfur mustard and is also used as an antioxidant for the chromatography of amino acids, in processes related to the determination of exposure to sulfur mustard and as a matching index fluid for quantitative imaging of concentrated suspensions of particles [42]. TDE is miscible in water, acetone, alcohols and chloroform [43].

1.3.3.3.2 Candidates for mounting medium based on TDE

As stated before, TDE accomplishes the characteristics of the optimal mounting, but it is not recommended when staining f-actin with fluorophores conjugated to phalloidin; also, the original report shows a limited compatibility of TDE with cells expressing green fluorescent proteins (GFP) [37]. Therefore in order to maintain the best features of TDE and obtaining also the possibility of working with phalloidin, some molecules have been chosen based on their specific similarity to TDE to assess if they would show improved performance with phalloidin conjugates, preserving the optical properties of the original medium.

The work presented in this thesis corresponds to the first stage of this project, in which four different molecules were considered: three commercially available 3,3'-thiodipropanol, 2,2'-sulfonyldiethanol (SDE) and butyl sulfone (BS), and a non-commercial compound, bis(2-methoxyethyl)sulfane. These molecules were considered as candidates because of their structural similitude to TDE. The structure of the commercial compounds chosen as candidates are represented in Table 2. On line 1 TDE structure is shown, on line 2 TDP, which has one additional carbon on each side of the chain, so that the longer chain could avoid interactions between the sulfur of the mounting medium molecule and phalloidin; on line 3 SDE, which has two oxygen atoms trapping the sulfur; and in line 4 BS, which lacks the OH at the two sides of the chain. Bis(2-methoxyethyl)sulfane has the same length and the sulfur exposed but has the final OH blocked.

TDP, is used in the determination of TDE in groundwater by a highly sensitive analytical method, SDE is used as a cross-linking agent for poly(vinyl phosphonic acid) (PVPA); both are yellowish to colorless liquids miscible in water.

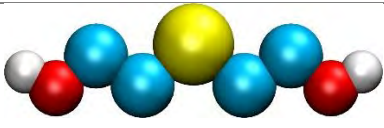

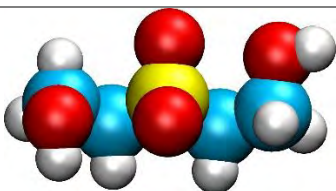
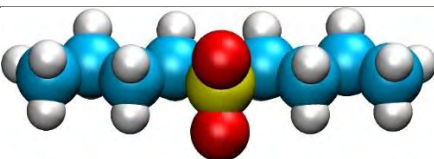
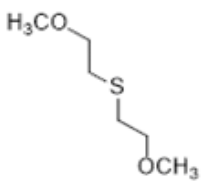
	Molecule CAS number	Chemical structure and formula	Density	Refractive index
1	2,2'-thiodiethanol TDE 111-48-8	 C ₄ H ₁₀ O ₂ S	1.221 g/mL at 25 °C	n _D =1.5189
2	3,3'-thiodipropanol TDP 10595-09-2	 C ₆ H ₁₄ O ₂ S	1.092 g/mL at 25 °C	n _D =1.506
3	2,2'- sulfonyldiethanol SDE 2580-77-0	 C ₄ H ₁₀ O ₄ S	1.236 g/mL at 25 °C	n _D =1.429
4	butyl sulfone BTS 598-04-9	 C ₈ H ₁₈ O ₂ S	Not given	Not given
5	Bis(2-methoxyethyl) sulfane Not commercial	 C ₆ H ₁₄ O ₂ S	Not given	Not given

Table 1.4 shows the chemical structure of TDE and the three molecules first considered as possible mounting media, their densities and refractive index [44].

BS is sold as crystals and for our purpose we needed to dissolve them in water. In order to solubilize BS we tried three different ways. First, the crystals were immersed in water at different concentrations and stirred with a magnetic stirrer at room temperature, but results were not satisfactory, some flocculation formed at the top and bottom of the test tube. Next we put the recipient with the compound into an ultrasonic bath for 5 hours in periods of an hour, 5 times, but the results were not satisfactory either: even though some crystals reduced their size; no solubilization was achieved. Eventually, the container with the crystals and water previously described was heated in a thermal bath to increase solubility. The only result was that micellae formed when the mixture reached the temperature of 40°C. Therefore, BS was eliminated from candidates list because it is not soluble in water, making it impossible to be used as a mounting medium.

The synthesis of Bis(2-methoxyethyl)sulfane is patented (EE.UU. 3095457,1963) and the procedure described in the patent has been followed by Dr. Rodriguez and coworkers to obtain it: metal sodium was placed into a flask and methanol was added, it was stirred for 30 minutes under nitrogen atmosphere. Thereafter, 3,3-thiobis (propanol) was added; the mixture was kept under stirring and at reflux temperature for 24 hours. The advance of the reaction was studied by thin layer chromatography using mobile phase hexane: ethyl acetate (8: 2). Under these reaction conditions it was not possible to obtain the compound; the possibility of obtaining the synthesis with the use of a prolonged reflux or microwave time will be evaluated in a successive stage of the project.

Eventually, four different mounting media have been used in this work: ProLong Diamond (PLD), 2,2'-thiodiethanol, 3,3'-thiodipropanol and 2,2'-sulfonyldiethanol .

PLD and TDE are known mounting media for fluorescence microscopy, but TDP and SDE have been tested in this work.

TDE is viscous and therefore requires incubation steps before mounting. Water will leave cells quicker than TDE will go inside them because of the difference in viscosity between these two media. When TDE is used at 97% the difference is large enough to produce cell shrinkage, then so a stepwise protocol must be followed to mount cells using TDE.

Incubations with increasing concentrations of mounting medium (10%, 25%, 50%, and 97%) are necessary before mounting, in this work they will be called pre-mounting incubations. Finally a 97% concentration is used to incubate for three times to assure homogeneous refractive index on the sample [37]. TDP and SDE used the same protocol.

1.3.4 Actin cytoskeleton, our structure of interest

The cytoskeleton is the structure that maintains cell shape and its internal organization, in fact mechanical integrity of a cell depends on it and also many essential functions like division and movement.

It is formed by three major filamentous structures different in size and by the cytoplasmic proteins that polymerize to constitute them. Microtubules are made up of tubulin and they are the filaments with the largest diameter, 25 nm; microfilaments containing actin are the thinnest with a 7 nm diameter and intermediate filament containing keratin-like proteins are between 8 and 12 nm [45]. And if compared to other cell proteins the cytoskeletal proteins are very abundant because they form very extended networks in cells [46].

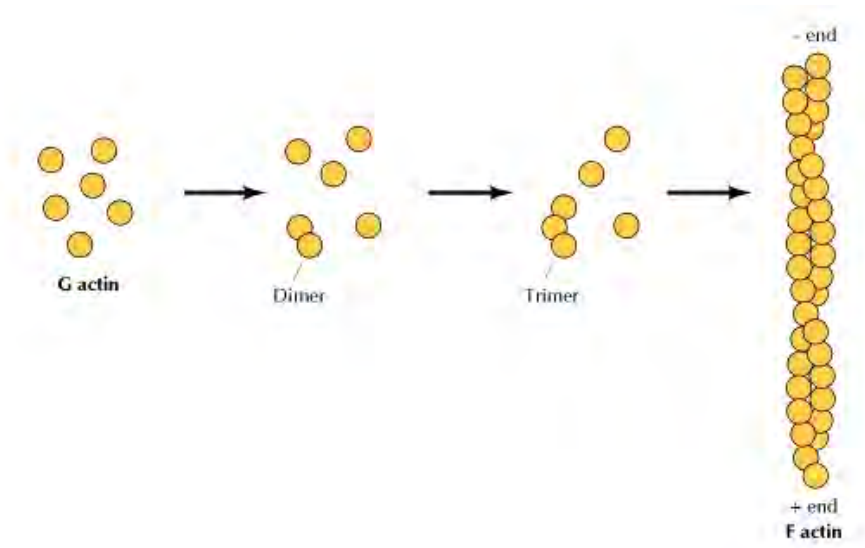


Figure 1.9 Assembly of actin filaments. Actin monomers polymerize to form actin filaments. Dimers and trimers are the first to be formed, then monomers add to both ends.

Actin is a protein present in all eukaryotic cells, especially in muscle and the microvilli of intestinal epithelial cells. It is present as globular monomers called G-actin and filamentous polymers called F-actin or microfilaments. A microfilament is a twisted double chain of actin subunits that form the actin cytoskeleton, a dynamic network of filaments, which main functions are maintenance of cell shape, changes of cell shape, muscle contraction, cytoplasmic streaming, cell motility and cell division. The network is dynamic because of the capability of G-actin to polymerize into F-actin and F-actin to depolymerize into G-actin rapidly. The assembly, length and stability of F-actin is regulated by actin binding proteins.

1.3.5 Staining the actin cytoskeleton

Staining actin cytoskeleton is a regular practice in biological laboratories either because of an interest on the structure itself, or as a counterstain, because visualization of actin filaments could give information on the cell's shape and health.

Phallotoxins are a group of bicyclic heptapeptides from poisonous mushroom *Amanita Phalloides* [47]. The most representative of this group is phalloidin. Phalloidin binds to filamentous actin and not to globular actin providing a better way to stain only the actin cytoskeleton with lower background than anti actin antibodies that will bind also to globular actin [48]. Another advantage respect to anti actin antibodies, is that binding of phalloidin to F-actin is not appreciably different between species, including plants and animals. In terms of procedures, phalloidin labeling requires less time and is more efficient than antibodies.

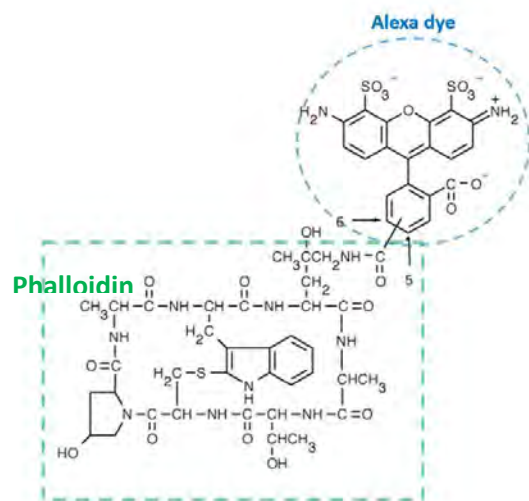


Figure 1.10 Chemical structure of phalloidin conjugated to AlexaFluor 488 dye [49].

There are other ways to stain actin, for example in live cells fluorescent actin or actin binding proteins could be used, although their insertion into the cell involve microinjection or the use of reagents for cell transfection. New products that serve the same purpose are SiR-Actin [50] and life act [51], life act is exclusively used in live cells and SiR-Actin has recently been reported to be suitable for the use in fixed cells.

Also compared to the use of fluorescent proteins the advantage of phalloidin is that the latter can be used in all cells but proteins cannot be expressed in all cell lines

and variations in efficiency of expression could be due to several variables, difficult to control.

1.4 Molecular dynamics simulation

The main goal of carrying out molecular simulations is modeling the real behavior of atoms based on intra- and intermolecular interactions. For this, we propose an adequate function that describes the interaction among atoms to calculate the force experienced as a function of positions of other atoms. Using this information, it is possible to determine the dynamic evolution of each atom along time, utilizing Newton's second law. This methodology is known as Molecular Dynamics (MD) and it is a tool widely used to study these systems to understand at an atomistic level different biological phenomena, like enzyme mechanisms and regulation [52].

In MD, time is divided into discrete steps. For each time step, forces acting on each atom are computed as a function of an effective intermolecular potential. And then, positions and velocities of atoms are updated using classical mechanics.

1.4.1 Molecular interactions

For a simple atomic system, we can relate the dynamic behavior with intermolecular interaction following equations:

$$m_i \mathbf{a}_i = \mathbf{f}_i, \quad \mathbf{f}_i = -\frac{\partial U}{\partial \mathbf{r}_i} \quad (1.8)$$

where \mathbf{f}_i is the force acting on the i -atom, $U(\mathbf{r}^N)$ is the potential energy and $\mathbf{r}^N = (r_1, r_2, \dots, r_N)$ represents the complete set of $3N$ atomic coordinates.

As velocity is the derivative of position, as well as acceleration is the derivative of velocity it can be written as:

$$\frac{d\mathbf{r}_i}{dt} = \mathbf{v}_i, \quad \frac{d\mathbf{v}_i}{dt} = \frac{\mathbf{f}_i}{m_i} \quad (1.9)$$

Differential equations that evolve the dynamics behavior of the system have not analytical solutions, a numerical method is implemented as follows:

$$r_{i+1} = r_i + \delta_t v_i, \quad v_{i+1} = v_i + \frac{\delta_t f_i}{m} \quad (1.10)$$

Where δ_t is the time step [53].

For this work, Groningen machine for chemical simulations (GROMACS) engine, has been chosen to perform molecular dynamics simulations.

1.4.2 GROMACS

“The GROMACS package is a versatile collection of programs and libraries for the simulation of molecular dynamics and the subsequent analysis of trajectory data. Although it is primarily targeted at biological molecules with complex bonded interactions, the very effective implementation of non bonded force calculations makes GROMACS suitable for all kinds of molecular dynamics simulations based on pair potentials” [54].

1.4.2.1 Units used in GROMACS

Quantity	Symbol	Unit
Length	r	$nm = 10^{-9} nm$
Mass	m	U (unified atomic mass unit) = $1.660538921 \times 10^{-27} kg$
Time	t	$ps = 10^{-12} s$
Charge	q	$e = elementary\ charge = 1.602176565 \times 10^{-19} C$
temperature	T	K

Table 1.5 Basic units used in GROMACS

1.4.2.2 Reduced units

In GROMACS is possible to use reduced units, represented commonly with an asterisk. To get this, input values must be given in these units. One exception is the temperature, which is expressed as 0.0083144621 in reduced units. Thus not T^* , but $k_B T$, is the reduced temperature. A GROMACS temperature $T^* = 1$ means a reduced temperature of 0.008 Units.

Quantity	Symbol	Relation to SI
Length	r^*	$r \sigma^{-1}$
Mass	m^*	$m M^{-1}$
Time	t^*	$T \sigma^{-1}$
Temperature	T^*	$K_B T \epsilon^{-1}$
Energy	E^*	$E \epsilon^{-1}$
Force	f^*	$F \sigma \epsilon^{-1}$
Pressure	P^*	$P \sigma^3 \epsilon^{-1}$
Velocity	v^*	$v \sqrt{\frac{M}{\epsilon}}$
Density	ρ^*	$N \sigma^3 V^{-1}$

Table 1.6 Reduced Lennard Jones quantities.

Lennard Jones potential:

$$V_{LJ} = \left[\left(\frac{\sigma}{r} \right)^{12} - \left(\frac{\sigma}{r} \right)^6 \right] \quad (1.11)$$

1.4.2.3 Periodic boundary conditions

Periodic boundary conditions are applied, in finite systems, in order to minimize edge effects. The atoms of the system to be simulated are put into a space-filling box,

which is surrounded by translated copies of itself. According to the system under study different shapes for space-filling unit cells could be preferred. GROMACS is based in triclinic unit cell because they are the most general space-filling unit cells that comprise all possible space filling shapes. GROMACS uses periodic boundary conditions, combined with the minimum image convention: only the nearest image of each particle is considered for short-range non-bonded interaction terms. For long-range electrostatic interactions GROMACS incorporates lattice sum methods such as Ewald Sum and PME. GROMACS supports triclinic boxes of any shape.

1.4.2.4 Cut-off restrictions

For non-bonded interactions the minimum image convention implies that the cut-off radius may not exceed half the shortest box vector, otherwise more than one image would be within the cut-off distance of the force.

1.4.3 The global MD algorithm

A global algorithm to simulate a system in the framework of the molecular dynamics is described as follow:

1. To define initial conditions

- Intra- and Intermolecular interactions as a function of atom positions.

- Positions r of all atoms in the system

- Velocities v of all atoms in the system

Repeat 2,3,4 for the required number of steps.

2. Compute forces

- The force on any atom:

$$f_i = -\frac{\partial U}{\partial r_i} \quad (1.12)$$

this is computed by calculating the force between non-bonded atom pairs:

$$f_i = \sum_j f_{ij} \quad (1.13)$$

Plus the forces due to bonded interactions (which may depend on 1, 2, 3 or 4 atoms), plus restraining and external forces.

The potential and kinetic energies and the pressure tensor may be computed.

3. Update configuration

The movement of the atoms is simulated by numerically solving Newton's equations of motion.

$$\frac{d\mathbf{r}_i}{dt} = \mathbf{v}_i, \quad \frac{d\mathbf{v}_i}{dt} = \frac{\mathbf{f}_i}{m_i} \quad (1.14)$$

4. If required: Output step

Write positions, velocities, energies, temperature, pressure, etc.

Integration algorithms

GROMACS allows the user to choose from two integrators for integrating Newton's equations of motion, the Leap-frog algorithm and velocity Verlet algorithm. Leap-frog algorithm is the integrator by default and when extremely accurate integration with temperature and/or pressure coupling is required, the velocity Verlet integrators may be preferable.

Leap frog algorithm uses positions \mathbf{r} at time t and velocities \mathbf{v} at time $t - \frac{1}{2}\delta_t$; it updates positions and velocities using the forces $\mathbf{f}(t)$ determined by the positions at time t , using these relations:

$$\mathbf{v}\left(t + \frac{1}{2}\delta_t\right) = \mathbf{v}\left(t - \frac{1}{2}\delta_t\right) + \frac{\delta_t}{m}\mathbf{f}(t) \quad (1.15)$$

$$\mathbf{r}(t + \delta_t) = \mathbf{r}(t) + \delta_t\mathbf{v}\left(t + \frac{1}{2}\delta_t\right) \quad (1.16)$$

The algorithm produces trajectories that are identical to the Verlet algorithm, whose position-update relation is

$$\mathbf{r}(t + \delta_t) = 2\mathbf{r}(t) - \mathbf{r}(t - \delta_t) + \frac{1}{m}\mathbf{f}(t)\delta_t^2 + O(\delta_t^4) \quad (1.17)$$

The algorithm is of third order in r and is time-reversible.

Velocity Verlet algorithm uses positions r and velocities v at time t to integrate equations of motion; velocities at previous half step are not required.

$$\mathbf{v}\left(t + \frac{1}{2}\delta_t\right) = \mathbf{v}(t) + \frac{\delta_t}{2m}\mathbf{f}(t) \quad (1.18)$$

$$\mathbf{r}(t + \delta_t) = \mathbf{r}(t) + \delta_t\mathbf{v}\left(t + \frac{1}{2}\delta_t\right) \quad (1.19)$$

$$\mathbf{v}(t + \delta_t) = \mathbf{v}\left(t + \frac{1}{2}\delta_t\right) + \frac{\delta_t}{2m}\mathbf{f}(t + \delta_t) \quad (1.20)$$

If used without pressure or temperature coupling both algorithm will give identical trajectories.

1.4.5 Force field

A force field is a mathematical expression that uses particle's coordinates of a system to describe its energy. It is a functional form and a set of parameters used to calculate the potential energy of a system of atoms or coarse grained particles in molecular mechanics and molecular dynamics simulations.

The parameters are typically obtained either from ab initio or semi-empirical quantum mechanical calculations or by fitting to experimental data such as neutron, X-ray and electron diffraction, nuclear magnetic resonance, infrared, Raman and neutron spectroscopy, etc.

The force field replaces the true potential of molecules with a simplified model that must be valid in the region being simulated.

GROMACS supports different force fields, between them are GROMOS 96, optimized potential for liquid simulations all atom (OPLS/AA), Assisted Model Building with Energy Refinement (AMBER), chemistry at Harvard macromolecule mechanics (CHARMM), coarse grain force fields, among others.

1.4.6 Potential energy

The functional form or potential energy in molecular mechanics include bonded and non bonded terms, for covalent bonds and long range interactions, respectively.

In GROMACS, the potential functions can be subdivided into three parts

1. Non-bonded: Lennard-Jones or Buckingham, and Coulomb or modified Coulomb. The non bonded interactions are computed on the basis of a neighbor list (a list of non-bonded atoms within a certain radius), in which exclusions are already removed.
2. Bonded: covalent bond-stretching, angle-bending, improper dihedrals, and proper dihedrals. These are computed on the basis of fixed lists.
3. Restraints: position restraints, angle restraints, distance restraints, orientation restraints and dihedral restraints, all based on fixed lists.

Common energy functions

$$\begin{aligned}
U &= \sum_{bonds} \frac{1}{2} k_r (r - r_0)^2 && \text{Bond stretches} \\
&+ \sum_{angles} \frac{1}{2} k_\theta (\theta - \theta_0)^2 && \text{Angle bending} \\
&+ \sum_{torsions} \frac{V_n}{2} [1 + \cos(n\phi - \delta)] && \text{Torsional rotation} \\
&+ \sum_{improper} V(improper\ torsion) && \text{Improper torsion (sp2)} \\
&+ \sum_{elec} \frac{q_i q_j}{r_{ij}} && \text{Electrostatic interaction} \\
&+ \sum_{LJ} \left[\frac{A_{ij}}{r_{ij}^{12}} - \frac{B_{ij}}{r_{ij}^6} \right] && \text{Lennard-Jones interaction}
\end{aligned}$$

Materials and methods

2.1 Mounting Media

One of the requirements in eukaryotic cell biology is maintenance of the osmotic equilibrium, then it is preferable that all processes related with cell slides preparation for imaging are performed with media of the same osmolarity. The mounting media used in this work were prepared using phosphate buffered saline (PBS) as solvent, when needed. The use of PBS helps maintaining the osmolarity and also adequate pH value for cell slide preparations. On the other hand each dye has a particular pH range in which it performs better. Both considerations may be taken into account for pH adjustment of mounting media.

For preparation, 2,2'-thiodiethanol (CAS 111-48-8, No. 166782 Sigma-Aldrich), 2,2'-sulfonyldiethanol (CAS 2580-77-0, No. 180084 Sigma Aldrich) and 3,3'-thiodipropanol (CAS 10595-09-2, No. 205346 Sigma Aldrich) were adjusted to pH \sim 7.5 with sodium hydroxide. The initial pH of these media depended on the purity of each batch and therefore was determined each time a new bottle of product was acquired.

In order to obtain 1 mL of TDE mounting medium, 970 μ L of TDE (already pH adjusted) and 30 μ L of PBS were mixed; the solution had a refractive index of $n_e^{23} = 1.515$, as described by Staudt et al. SDE and TDP only needed pH adjustment because their refractive indices at their highest concentration were lower than the ideal 1.518.

The above mentioned are the final solutions used in the mounting process. Three other solutions at 10%, 25% and 50% concentration, were used to incubate the

samples. Table 2.1 shows the volumes of medium, water and PBS used in case of preparation of 1 mL of each mounting medium

Para 1mL	TDE/TDP/SDE (uL)	PBS 1X (uL)	H₂O (uL)
10%	100	250	650
25%	250	250	500
50%	500	250	250
97%	970	30	0

Table 2.1 Volumes used to make incubation solution for the mounting process of slides. Column 2 refers to either TDE, TDP or SDE on each case.

2.2 pH adjustment

Three different methods were used to measure and adjust pH value. The first was to use a Jenway pH/mV Temperature Meter Model 3510 (Cole-Parmer, UK). The high viscosity of the medium did not allow NaOH to mix properly and the pH values measured kept changing over hours.

The second method was using pH indicator strips (Macherey Nagel); this method together with the third one, consisting in the use of the chromometric pH indicator phenol red (No. P4758, Sigma Aldrich) allowed us to set pH of media around 7.4. The original pH of TDE was 5, of TDP 4 and SDE 4.

In order to determine pH using the chromometric indicator it is necessary to know the color of the desired pH. To do so, five solutions with known and different pH values were prepared, to establish the color appearance of each pH value. 1mL of solution with known pH was mixed with 10 uL of phenol red working solution. The phenol red working solution is 4.1 mg/mL. With this concentration, 10 uL of phenol red in a sample of 1 mL was enough to establish the pH value by differences of color.

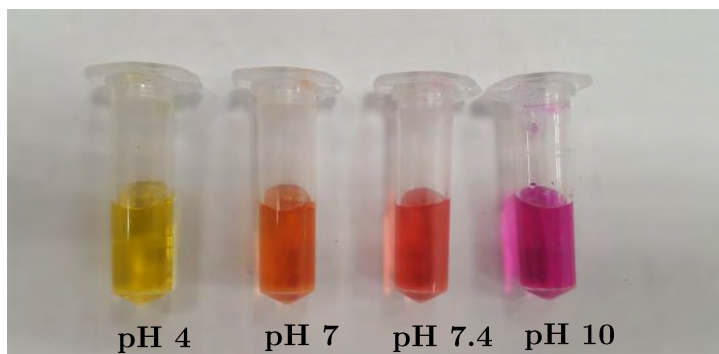


Figure 2.1 Calibration solutions of different pH values colored with phenol red.

In the same way, that is, mixing 10 uL of phenol red to 1 mL of medium, the original pH of the media was measured. Additionally the pH was also verified by the use of pH indicator strips.

Then, NaOH was added dropwise to 1mL of original medium (either TDE, TDP or SDE) to obtain the right pH value, by adjusting the color to that of samples of 7 and 7.4 pH. To prepare the pH-adjusted media, the above defined amounts of NaOH, used previously to obtain the proper color, were directly added to the media.

Medium volume	Initial pH	NaOH concentration and volume	Final medium volume	Final pH
TDE 1.5 mL	5	0.05 M, 3 uL	15003 uL	7.5
TDP 1 mL	5	2 M, 4 uL	1004 uL	7
SDE 1 mL	4	2 M, 52 uL	1052 uL	7

Table 2.2 Volumes of NaOH used to adjust pH of media.

2.3 Refractive index measurement

When light interacts with matter, it reflects and refracts, being its refraction angle dependent on the refractive index of the material and variable with the wavelength.

Shorter wavelengths refract at lower angles, respect to the normal to the interface, compared to larger wavelengths of visible light. We have measured the refractive indices of TDE and TDP in the range from 480 nm to 680 nm, and compared them with those of immersion oil.

Refractive indices of TDE, TDP, VectaShield (Vector Labs, Product number H 1000) and immersion oil Immersol 518 F(**Item Number:** 444960-0000-000) were measured with an Abbe refractometer Type-WY1A (Edmund Optics, Barrington, U.S.A.). The beam used as illumination source was a supercontinuum Laser SCT 500 (FLYA, Valencia, Spain). The laser beam was spatially separated using a monochromator MC1-01 (Optometrics, Ayer, U.S.A.). The data were measured every 10 nm, starting from 480 and ending at 680 nm. Additionally, n_D (589 nm) and n_e (546 nm) were measured as they are commonly used to express n values for various materials.

The supercontinuum laser used has a spectral range that starts at 500 nm and ends at 2150 nm. The output power varies with the wavelength: at the used spectral band the power was >10 mW and total power (full spectrum) >500 mW. The laser repetition rate is 20 MHz, and its fundamental pulse width 20 ps. The white beam of light generated by supercontinuum laser was spatially separated into component wavelengths, with a monochromator that consists of three mirrors and a grating (Figure 2.2 d).

To convert the narrow beam of light exiting from the monochromator to a broad beam filling the surface of the illumination prism for measuring the refractive index, a 10X objective was inserted in the light path between the slit and the refractometer.

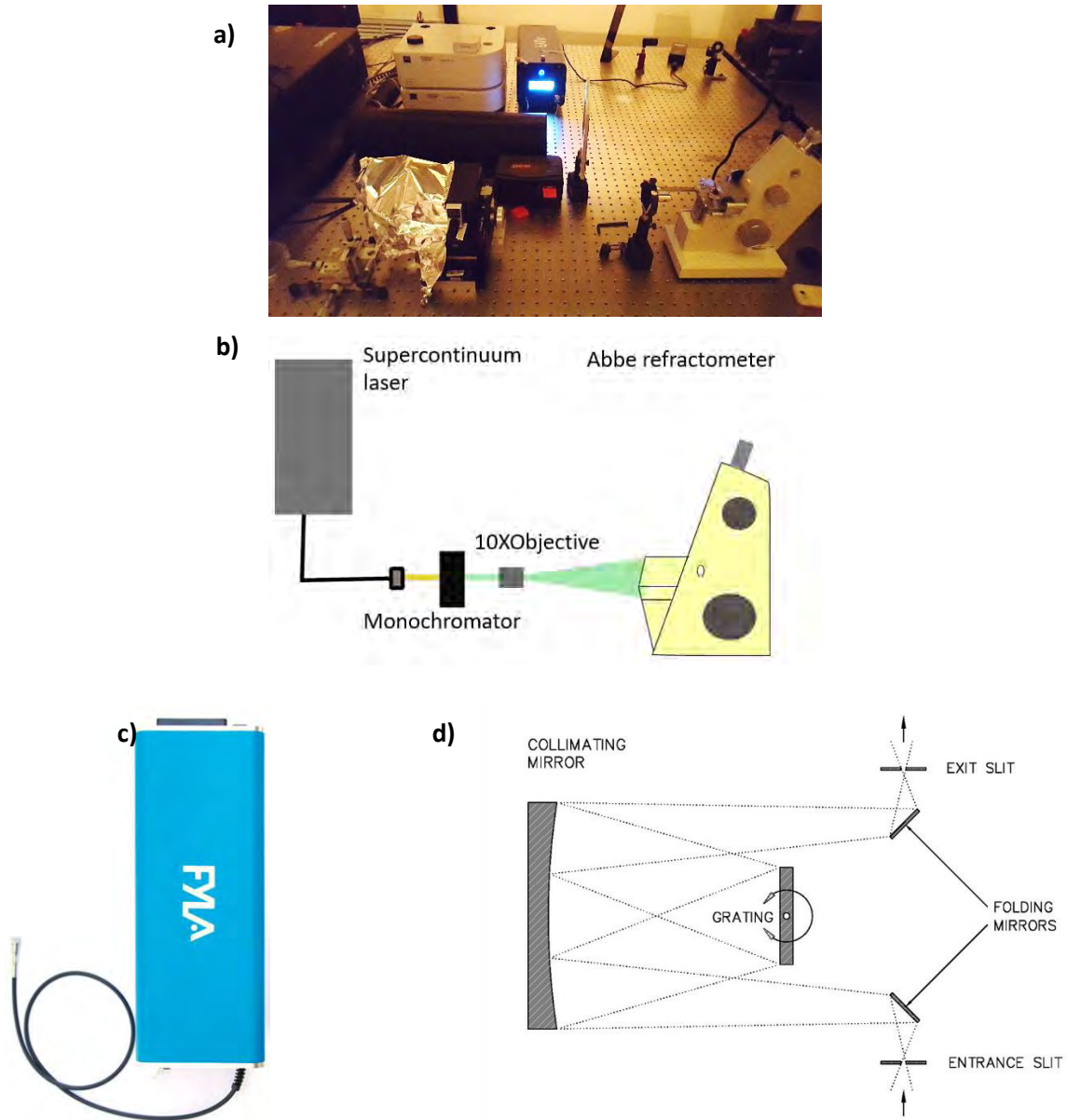


Figure 2.2 a) Experimental set up used to measure refractive indices at different wavelengths. The supercontinuum laser was spatially separated using a monochromator and a 10X objective was used to expand the beam. b) The supercontinuum laser used, and c) the optical diagram of the monochromator [55].

The Abbe refractometer is designed to measure the refractive index of transparent solids and liquid samples using total internal reflection. The critical angle for the interface between the specimen and the refracting (measuring) prism in the

refractometer is measured and, according to this, the refractive index of the sample can be obtained. As is shown in Figure 2.3 diffuse light passes through the illumination prism and reaches the interface with the specimen from different angles, respect to the normal to the interface.

If the incident angle is wider than the critical angle then total reflection occurs at the interface, and no light is transmitted into the specimen (dotted lines). If the incident angle is narrower than the critical angle, light is transmitted. At an angle δ the transition from transmission to total reflection occurs and that is why the image shows a defined separation between illuminated and dark range (full lines). By changing the observation angle it is possible to adjust the line that separates illuminated from dark range to the point of intersection of a reticle and read a value, corresponding to the measured refractive index, from a scale.

Experimental data was fitted to Cauchy's dispersion equation using the program OriginPro 9.0. First, the linear fitting was performed, using the lineal form of the one term Cauchy's equation $n = B_0 + B_1\lambda^{-2}$. After obtaining the values of B_0 and B_1 , a nonlinear fitting was used for the data. The equation used for the non-linear fitting was $n = B_0 + \frac{B_1}{\lambda^2} + \frac{B_2}{\lambda^4} + \frac{B_3}{\lambda^6}$. The parameters B_0 and B_1 were used as the initial value for the non-linear fitting process.

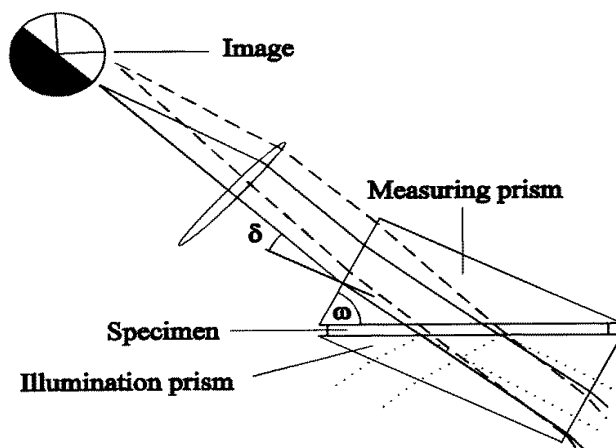


Figure 2.4 The working principle of an Abbe refractometer [56].

2.4 Fluorescence dyes

The following fluorophores were used in the spectroscopic measurements, Alexa Fluor 488 phalloidin (Thermo Fisher Scientific, No A12379), Alexa Fluor 647 phalloidin (Thermo Fisher Scientific, No A22287), DAPI (Thermo Fisher Scientific, No 62248) and Rose Bengal (No. 198250, Sigma Aldrich).

2.5 Spectra measurements

Absorption and emission spectra of the dyes dissolved in TDE, TDP and PBS were recorded in order to define if there was a spectral shift due to solvatochromism of the dyes.

Also the maximum intensity in both spectra was measured for the probes in TDE, TDP and PBS to obtain a relative quantum yield (QY_{Rel}). This QY_{Rel} is a comparison between intensities of emission and absorption for the probes in TDE and TDP compared to the same in PBS, being the equation that describes this relation:

$$QY_{Rel} = \frac{Abs_{PBS}}{Abs_{TDX}} \cdot \frac{Em_{TDX}}{Em_{PBS}} [37].$$

Probe	DAPI	Alexa Fluor 488 phalloidin	Alexa Fluor 568 phalloidin	Alexa Fluor 647 phalloidin	Rose Bengal
Sub-cellular localization	Nucleic acids, nucleus	Actin, cytoskeleton	Actin, cytoskeleton	Actin, cytoskeleton	Cytoplasm
Excitation/Emission (nm)	358/461 in water/DNA	495/517 at pH 7	578/600 at pH 7	649/666 In MeOH	546/550
MW	350.25	~1320	~1590	~1950	973.67
Extinction Coefficient	24 000	78 000	88 000	275 000	>90 000
Quantum Yield	0.34 *	0.92	0.69	0.33	0.11
Lifetimes (ns)		4.1	3.6	1	
Notes	1	2,3	2,3	2,3,4.	

Table 2.3 Specifications given by ThermoFisher Scientific for these products [57].

*Bound to DNA and is 20 folds the quantum yield (QY) value in water.

1. Abs/Em in water 342/454.
2. Phallotoxins conjugates have approximately 1 label per peptide.
3. The value of extinction coefficient (EC) is for the labeling dye in solution. Use of this value for the conjugate assumes a 1:1 dye peptide labeling ratio and no change of EC due to dye peptide interactions.
4. In aqueous solution (pH 7.0), Abs/Em= 649/666 nm.

QY and lifetimes are given for the dyes and were obtained in PBS at 22°C, relative to fluorescein in 0.01 M NaOH (QY=0.92)

The absorption and emission spectra were measured with a Cytation 5 spectrophotometer (Biotek, Vermont, U.S.A.): suspensions of fluorophores in TDE, TDP and PBS were placed and measured within single wells of a black-walled, clear-bottom 96-well microplates (Corning Incorporated, NY, U.S.A.). Alexa Fluor phalloidin probes were used at a concentration of 2.6 uM and DAPI at 11.4 mM, Rose Bengal at 7.86 uM. The volume used in each measurement is 100 uL.

2.6 Cell culture and immunocytochemistry

Biological markers used are: anti-tubulin polyclonal primary antibody (sheep host) (Cytoskeleton, No. ATN02), monkey anti sheep secondary antibody conjugated to Alexa Fluor™ 488 (Thermo Fisher Scientific, No. A-11015), DAPI for the nucleus (Thermo Fisher Scientific, No 62248) and Alexa Fluor™ 488 phalloidin (Thermo Fisher Scientific, No A12379), Alexa Fluor™ 647 phalloidin (Thermo Fisher Scientific, No A22287) and Alexa Fluor™ 568 phalloidin (Thermo Fisher Scientific, No A12380) for F-actin.

Three cell lines were used: HEK 293, SH-SY5Y and HeLa. In this work cells have been stained for tubulin, F-actin and nucleus.

2.6.1 Culture method

Complete growth medium: The base medium for HEK and HeLa cells is Dulbecco's modified Eagle medium (DMEM) and for Sh-sy5y is DMEM F-12. The complete growth medium has fetal bovine serum to a final concentration of 10% and 100 U/mL of penicillin and 100ug/mL of streptomycin.

Subculturing: Volumes are given for a 25 cm^2 flask.

1. Remove culture medium in case of HEK293 and HeLa, and save in case of Sh-sy5y.
2. Add PBS to rinse and discard.
3. Add 0.8 mL of trypsin solution, place at 37°C for 1 minute in case of HEK293, 2 minutes in case of HeLa and Sh-sy5y.
4. Add 5 mL of complete growth medium and aspirate cells by gently pipetting.
In case of sh-sy5y, add the medium removed in step 1.

5. Centrifuge at 95 xg for 3 minutes. Discard the supernatant.
6. Add 4 mL of medium to the new flask.
7. Suspend the centrifuged cells in 4 mL of medium, take 0.5 mL and add to a new flask.
8. Incubate cultures at 37°C. Subculture when cell confluency is about 80-90%.

Cryopreservation: Freeze medium is complete growth medium supplemented with 5% (v/v) DMSO and storage temperature is liquid nitrogen vapor phase

Culture conditions: Atmosphere is composed of air, 95%; carbon dioxide (CO₂), 5% at a temperature of 37°C.

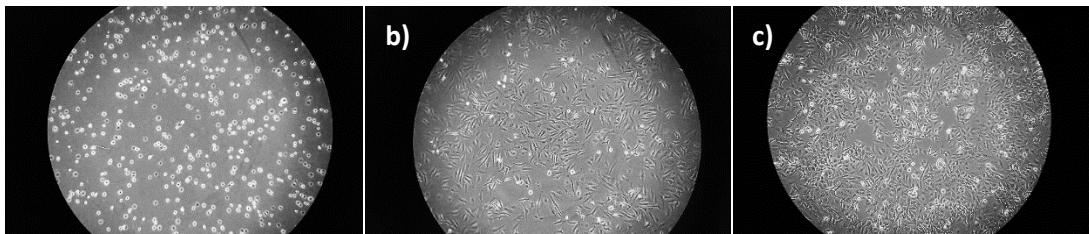


Figure 2.5 Phase contrast images of HeLa cells in adherent culture. The images were obtained using 10X objective, a) right after subculturing, b) one day after subculturing ~60% confluency, d) two days after subculturing ~80% confluency.

2.6.2 Fixation Method

Cells were subcultured in dishes containing coverslips so adherent cells attached to them. For optimal imaging cells should be ~70-80 % confluent. Formaldehyde is diluted in PBS to a final concentration of 4%.

Fixation: Add 4% formaldehyde on the dish containing the same volume of growth medium so that the final concentration is 2% formaldehyde and incubate for 15 minutes. Aspirate the solution, then add formaldehyde 2% in PBS and incubate for 15 minutes. Aspirate the solution, then wash with PBS.

Permeabilization: Remove PBS and add 0.1 % Triton X-100 in PBS for 10 minutes.

Blocking: Remove PBS-Triton and add blocking buffer composed of 10% bovine serum, 0.04% Triton X-100 in PBS for 30 minutes.

2.6.3 Staining method

Staining process was done in a humidified chamber. In a closed recipient, wet paper was placed at the bottom, with parafilm above it. Coverslips were moved to this humid chamber and placed upside down over 40 uL drops of media, and incubated in the dark.

1. Immunostaining: Incubate every coverslip upside down over a 40 uL, 1:500 dilution of primary antibody in blocking buffer at room temperature (RT) for 1h, or overnight at 4°C. Remove the antibody solution and wash three times with PBS at RT for 10 min each. Incubate with secondary antibody, at RT, in the dark, for 1h. Wash three times with PBS at RT for 10 min each wash.
2. F-actin staining: Incubate for 20 minutes in 0.132 uM Alexa Fluor phalloidin, at RT in dark. Wash three times with PBS at RT for 10 min each wash.
3. Nucleus staining: Incubate for 10 minutes in 2.855 uM DAPI, at RT in dark. Wash three times with PBS at RT for 10 min each wash.

2.6.4 Mounting

Mounting procedure for PLD:

Clean the glass slide and add the minimal volume of the mounting medium necessary to cover the entire cover slip. Remove coverslip containing the sample from PBS. Dry excess PBS from the cover slip by tilting the glass on an adsorbent paper. Place the coverslip cells down onto the mounting medium, avoiding bubbles. Seal the coverslip with transparent nail polish.

Four different mounting media were used in this work, PLD, TDE, TDP and SDE. When using TDE, TDP and SDE the procedure involved additional steps.

For 1mL	Mounting medium (uL)	PBS 1X (uL)	H2O (uL)
10%	100	250	650
25%	250	250	500
50%	500	250	250
97%	970	30	0

Table 2.4 1mL recipe of the different concentrations needed for incubations previous to mounting. In case of TDE mounting concentration is 97%, for TDP and SDE final concentration used is 100%.

The coverslips with cells were immersed for 10 minutes in increasing concentrations of the mounting medium: incubations were performed at 10% (mounting medium in PBS), then at 25% and at 50%. The final mounting was performed with 97% TDE, 100% SDE/TDP.

2.7 TDE effect on F-actin labeled with fluorescent phalloidins.

To explain the loss of fluorescence in cells labeled with phalloidins and mounted in TDE, two series of experiments were performed. One experiment thought to verify if TDE depolymerizes actin filaments already fixed. The other experiment designed to determine if fluorophores bonded to f-actin, loss their affinity when put in presence of TDE and got dissolved in the medium.

To observe if f-actin is depolymerized in presence of TDE, cells already fixed and permeabilized, were incubated in TDE. Incubation was performed in a stepwise manner increasing the concentration of TDE as usual, until 97% concentration was reached. Then cell were incubated for 24 hours in 97% TDE. With the same procedure, the cell slides were incubated in a reverse way to gradually reduce TDE concentration in cells. Then cells were washed in PBS for 30 minutes 4 times. Washing steps were performed with agitation, obtained with an orbital shaker to assure thorough mixing and facilitating diffusion. Following that, the staining with Alexa Fluor 488 phalloidin was performed as usual. Cell slides were mounted with PLD. The procedure was done in three different times and with many replications each opportunity. Finally six control slides and 24 experimental ones were obtained.

The second experiment was implemented under the assumption that, fluorescent phalloidins detach from f-actin when immersed in TDE, thus the probe is able to migrate outside the cell in presence of TDE. Cells were seeded in wells, the cells in wells were fixed, permeabilized and stained with Alexa Fluor 488.

As the idea is to understand if unbounded fluorophore leaves the cells and goes to TDE, and considering that the first contact cells have with TDE happens already during pre-mounting incubations, the pre-mounting incubations were performed in

wells. This way, the media containing TDE (pre-mounting incubation steps) removed from wells with cells were transferred to another well. Finally 97% TDE was added to cells and was left in incubation for 4 hours. 97% TDE was then removed and put into another well. The final amount of wells tested this way was 6 and other 6 were used as controls. 6 wells is an amount that gives enough statistic information considering the amount of fluorophore needed for the experiments. In the control experiment all steps described before were performed using PBS. PBS involved in incubation steps were similarly reserved in different wells.

Finally fluorescence from the wells with cells, the wells with incubation media and the wells containing the 4 hours incubation media, were measured. The experiment was done in sixfold.

2.8 Imaging

A LSM-710-NLO confocal microscope (Zeiss, Germany) equipped with LCI Plan-Neofluar 25x/0.8 Imm Korr DIC M27 and alpha Plan-Apochromat 63x/1.46 Oil Korr M27 immersion objectives were used for imaging.

The light sources used for imaging were: HeNe 543 laser for AlexaFluor 568, HeNe 633 laser for AlexaFluor 647, Argon laser (488 nm laser line) for Alexa Fluor 488 and 405 Diode laser for DAPI.

The three dyes conjugated to phalloidins used in this work were AlexaFluor 488, AlexaFluor 568 and AlexaFluor 647. They were used in combination with other probes as anti-tubulin AlexaFluor 488, DAPI and Hoescht, always limiting as possible the spectral overlap. The emission wavelengths for the detection and

acquisition window varied according to the fluorophores used in the sample and are given in Table 3.

Sample	Fluorophores	Excitation	Expected emission maximum	Detection wavelength range
1	AlexaFluor 488	488	561.5	493-630
	DAPI	405	455.5	410-501
2	AlexaFluor 568	543	640	568-712
	DAPI	405	497.5	410-585
3	AlexaFluor 647	633	696.5	638-755
	DAPI	405	497.5	410-585
4	AlexaFluor 488	488	548	494-601
	AlexaFluor 568	543	640	568-712
	DAPI	405	458	410-507
5	AlexaFluor 488	488	562.6	494-630
	AlexaFluor647	633	696.5	638-755
	DAPI	405	458.5	410-507
6	AlexaFluor568	543	640	568-712
	Hoescht	405	490.5	410-571
7	Alexafluor647	633	696	638-755
	Hoescht	405	490.5	410-571

Table 2.5 Acquisition mode parameters: channel excitation, emission and acquisition window for different combinations of fluorophores used.

Results

Mounting media are necessary and fundamental in microscopy for obtaining high quality biological images. Despite this, most of the commercially available media for fluorescence microscopy have far from ideal refractive index for high resolution fluorescence microscopy [39]. The higher resolution achievable with a microscope is obtained when the refractive index of the mounting medium matches that of the immersion liquid and the coverslip [58].

In order to find a substance that could perform as an ideal mounting medium, TDE has been chosen as the starting point for the search. TDE performs well with a variety of fluorophores, but could not be used with phalloidin-stained cells and tissues. The goal was to find a molecule that could be used as mounting medium and could also maintain the fluorescence of the actin cytoskeleton labeled with phalloidin. Based on this thiol, 4 candidates have been selected and their properties as mounting media have been studied in this thesis. Among them, the one with the highest refractive index, TDP, has also shown to maintain the fluorescence of F-actin in cells stained with phalloidin probes.

3.1 Refractive index of candidates for mounting media

An indispensable feature of the mounting media for high resolution fluorescent microscopy is their refractive indexes, so the refractive index of the 4 selected candidates were measured, and are shown in Table 3.1. TDE and TDP refractive indices provided on the web page of distributor are not in full agreement with the values we measured; the difference stems from the substantial variation in refractive

index among different lot numbers for the same product. In case of SDE the value is not given in supplier's page.

Molecule	TDE		TDP		SDE	
pH	5		5		4	
n_D^{20}	Vendor	Measured	Vendor	Measured	Vendor	Measured
	1.5215	1.5189	1.51	1.5060	1.42***	1.4290

Table 3.1 Refractive index of media provided by vendor or ***[59]. Experimental data measured in Abbe refractometer.

The refractive index for different concentrations of TDE, TDP and SDE were measured. Knowing the relationship between refractive index and mounting medium concentration is useful for tuning this value for experimental needs.

TDP is sold at purity >97%: the measurements correspond to a lot whose analysis indicates 99% purity. Then the 100% concentration showed here corresponds to the product purchased with the purity reported. In case of SDE, it is sold as solution in water, with a concentration between 60-65%. The concentration of SDE referred here as 100% corresponds to 60-65%.

Medium	Equation	Coefficient of determination	Residual sum of squares
TDE	$n = 0.00179C + 1.33682$	0.99514	0.00132
TDP	$n = 0.00172C + 1.33484$	0.99739	0.0003467
SDE	$n = 9.42588 \times 10^{-4}C + 1.33554$	0.99956	0.0000152815

Table 3.2 Parameters of linear fit obtained for data measured with Abbe refractometer.

The three compounds showed a linear behavior in refractive index value for increasing concentrations of the medium. For the linear fit: C stands for

concentration and n for refractive index. The measured refractive index corresponds to the sodium line at 23°C.

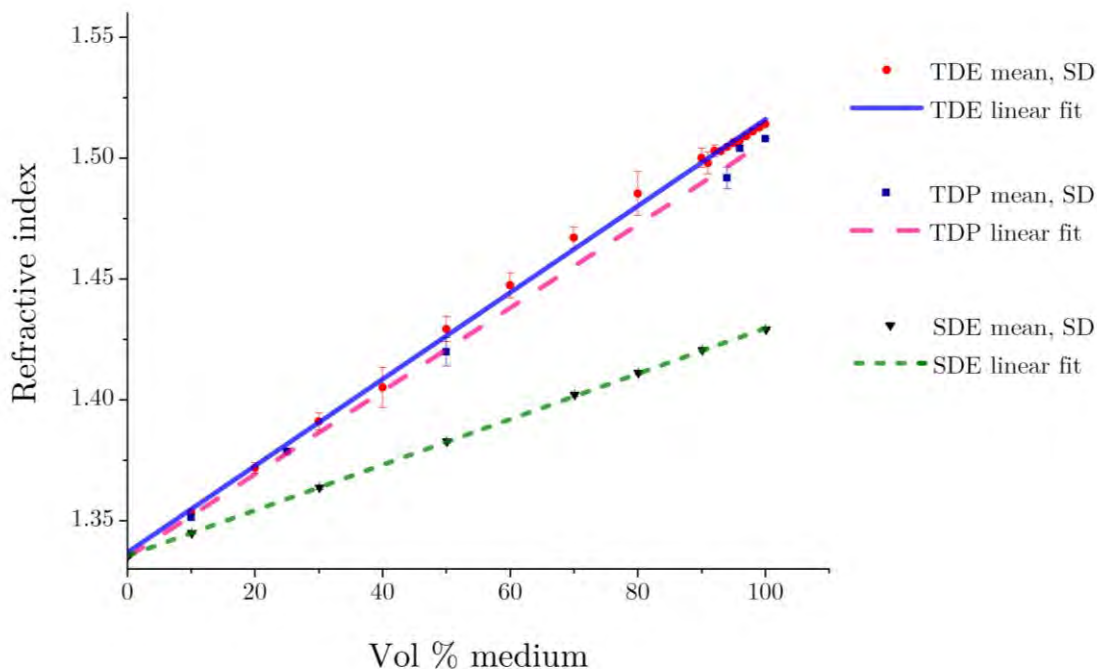


Figure 3.1 TDE, TDP and SDE are miscible in water. The refractive index of their solution can be precisely tuned to any value from 1.33 to 1.5145 for TDE, 1.508 for TDP and 1.429 for SDE. Mean value and standard deviation from measured data is shown in red dots and bars for TDE, blue for TDP and black for SDE.

3.2 Dispersion measurements

Refractive indices of oil immersion, VECTASHIELD, 97% TDE and TDP were measured from 480 nm to 680 nm. Two set of data points were obtained and were fitted to Cauchy's dispersion equation.

Cauchy's equation for dispersion was chosen because it provides a good fitting for dispersion in the visible range [60] [61].

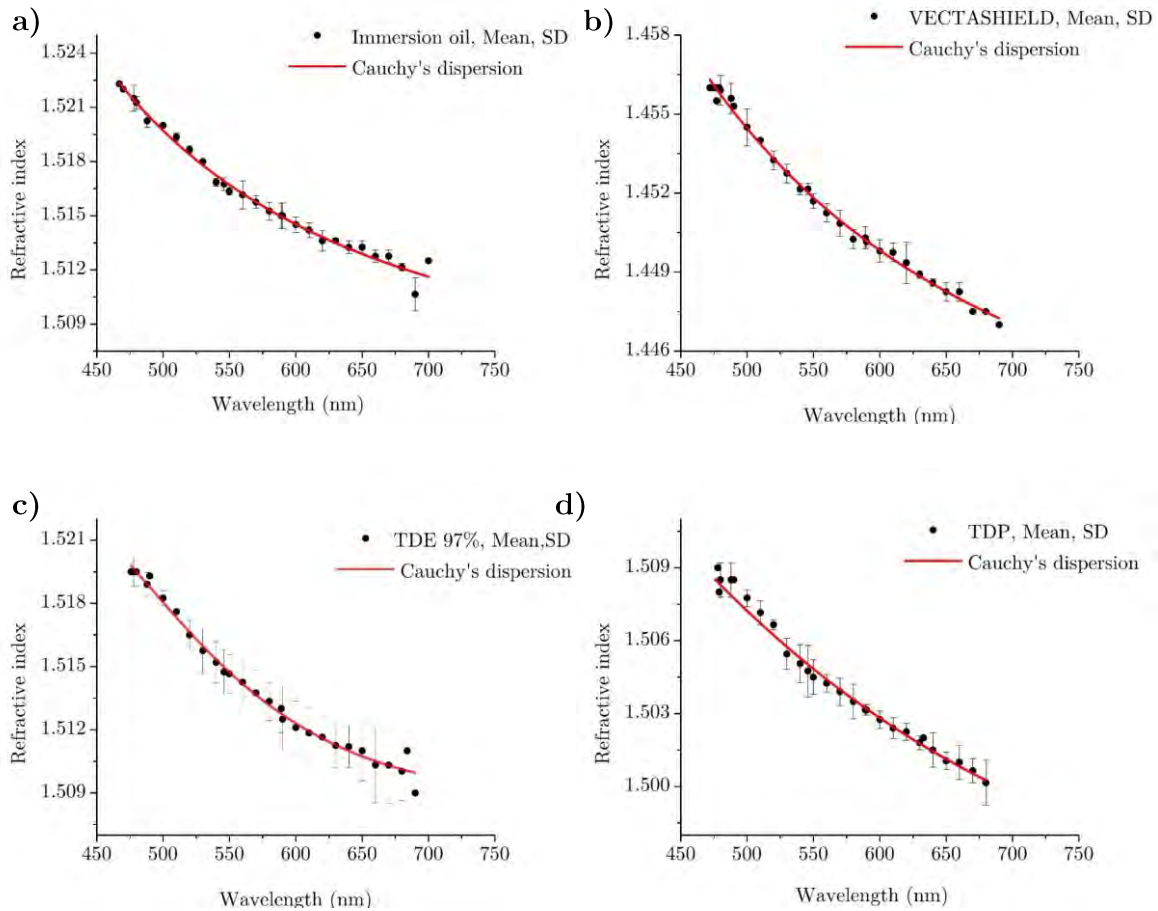


Figure 3.2 Dispersion curves of a) immersion oil, b) VECTASHIELD, c) 97% TDE, and d) TDP. Two set of experimental data were used in the fitting, both measurements were performed at 23°C with an Abbe refractometer.

In Figure 3.3, the dispersion curve of the immersion oil is shown together with those of the mounting media, because the ideal mounting medium should have RI dispersion that matches that of the immersion oil. The immersion oil is the liquid filling the space between the objective lens and the coverslip, then the closer the dispersion of the mounting medium is to that of the immersion oil the fewer the chromatic aberrations introduced by the mounting medium.

Parameters	TDE 97%	TDP	VECTASHIELD	Immersion oil
B_0	1.51621	1.48936	1.4392	1.50445
B_1	-10275.92366	5703.5341	3848.92341	3193.88511
B_2	4.35279×10^9	-3.0928×10^8	-8.69759×10^6	1.55428×10^8
B_3	-4.17241×10^{14}	1	1	1
R^2	0.940035	0.940022	0.988447	0.978820

Table 3.3 Constants of Cauchy's equation and coefficient of determination (R^2) for mounting media and immersion oil. The parameters correspond to curves in Figure 3.2.

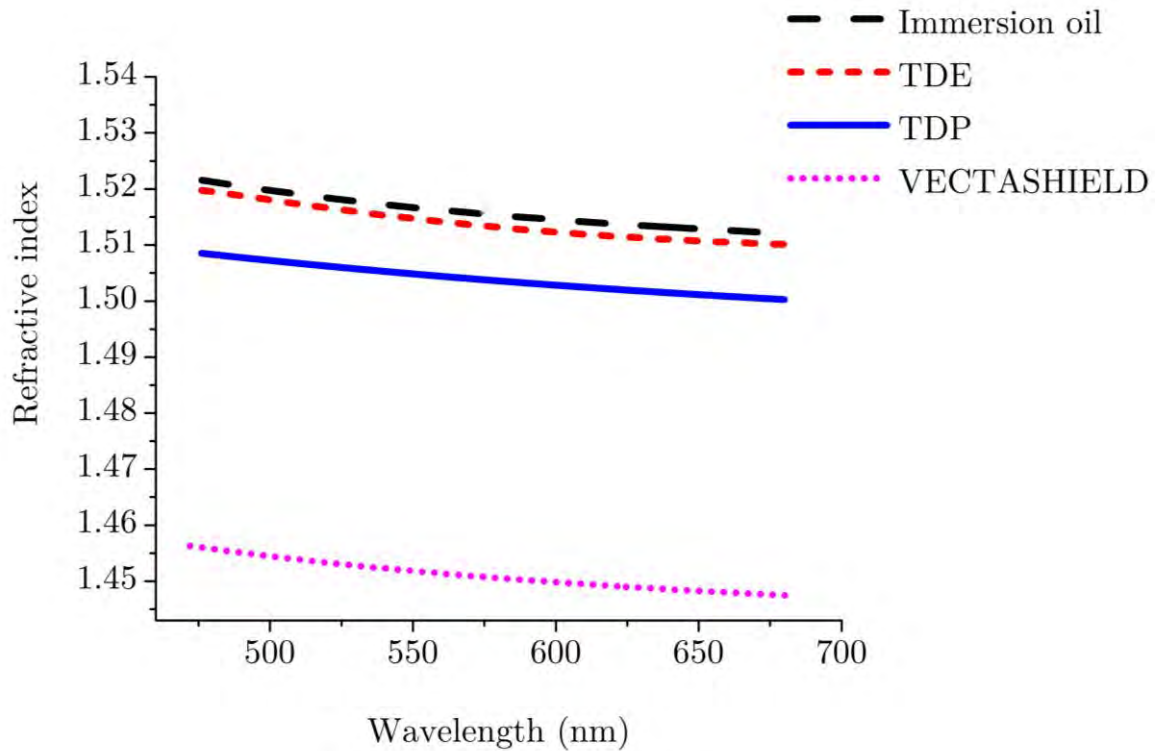


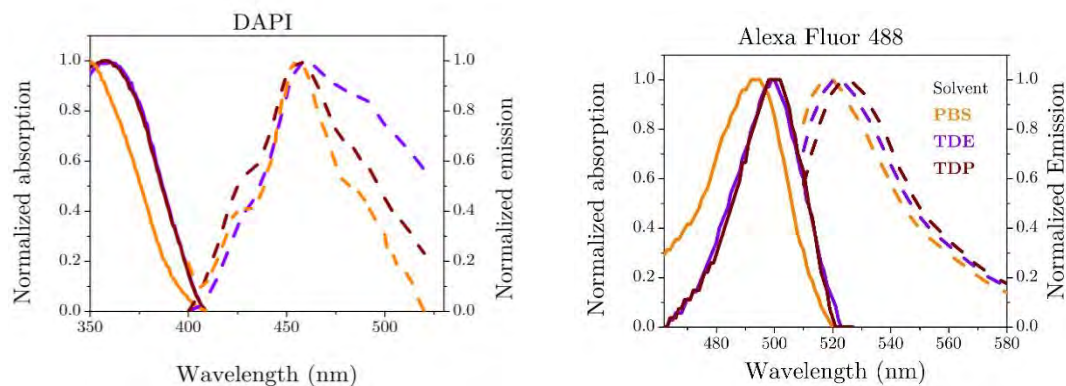
Figure 3.3 Dispersion of refractive index for immersion oil, TDE, TDP and VECTASHIELD. Curves correspond to Cauchy's equation $n = B_0 + \frac{B_1}{\lambda^2} + \frac{B_2}{\lambda^4} + \frac{B_3}{\lambda^6}$ with the parameters detailed in Table 3.3.

3.3 Absorption and emission spectra

To evaluate how the fluorescence of selected Alexa Fluor dyes and DAPI in PBS, TDE, and TDP could be generated and detected, the absorption and emission spectra of fluorophores has been measured in the 3 media. The results are summarized in Table 3.4 showing the maximum intensity of absorption and emission, the corresponding peak wavelengths and the relative quantum yield (Qy_{rel}). The data show that the fluorescence brightness is lower for Alexa Fluor 488 in TDE and TDP as compared to PBS. For Alexa Fluor 647 and DAPI fluorescence brightness is stronger.

For the three dyes, as expected, the absorption and emission spectra are altered by the solvents. The change in the spectra is due to solvent's polarity, and is called solvatochromism. The shift experienced for the three dyes correspond to a red shift, also called bathochromism.

Figure 3.4 shows the normalized absorption and emission spectra of dyes in the presence of PBS, TDE and TDP. The shift is also represented in Table 3.4 by the wavelength that corresponds to maximum of each one of the spectra.



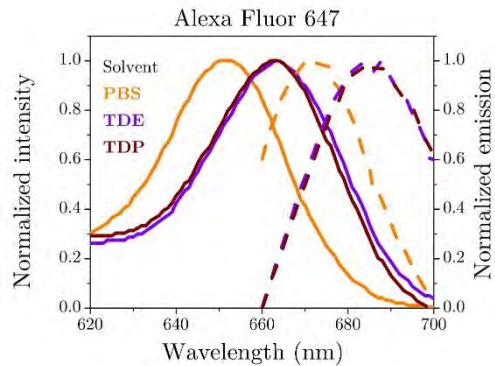


Figure 3.4. A red shift is observed when measuring the absorption (straight line) and the emission (dotted line) spectra of the three different dyes.

Knowing the solvatochromism of probes dissolved in the mounting media is important to determine excitation and detection wavelengths of the fluorescence microscope set up and detect if the excitation sources and filters, as well as the emission filters, are appropriate and efficient for the fluorescence of each experiment. For the confocal system that was used in this work, the excitation wavelengths were those recommended by the fluorophore vendors. The same excitation and emission parameters for a single fluorophore were used when imaging with PLD, TDE and TDP, as the mounting medium.

In Figure 3.5 the maximum intensity is shown for AF 488, AF 647, DAPI and Rose Bengal, dissolved in PBS, TDE and TDP. Spectra in PBS are the reference for comparison, because it is the solvent used in most staining procedures. In case of DAPI there is a red shift in absorption spectra, when dissolved in TDE and TDP, shorter than 19 nm. DAPI's emission spectra presents a shift of less than 7 nm. In case of AF 488 phalloidin there is a red shift smaller than 10 nm in absorption spectra, in TDE and TDP. The emission spectra are red shifted only for TDE. For AF 647 phalloidin there is a shift of less than 15 nm in absorption spectra for TDE

and TDP, and for the emission spectra the most pronounced shift is around 25 nm for TDE and TDP respect to PBS.

		DAPI	A488	A647
* Water pH 7	Abs. λ (nm)	342	495	649
	Em. λ (nm)	454	517	666
PBS pH 7.4	Abs. (a.u.)	0.107	0.06	0.099
	λ (nm)	360	494	652
	Em. (a.u.)	33785	49715	9886
	λ (nm)	458	520	672
TDE pH 4	Abs. (a.u.)	2.148	0.027	0.117
	λ (nm)	353	500	663
	Em. (a.u.)	67750	10357	14475
	λ (nm)	461	525	685
TDP pH 5	Abs. (a.u.)	0.155	0.037	0.084
	λ (nm)	358	500	664
	Em. (a.u.)	94680	11058	13168
	λ (nm)	455	522	684
QY_{relTDE}	$\frac{Abs_{PBS}}{Abs_{TDE/P}} \cdot \frac{Em_{TDE/P}}{Em_{PBS}}$	1.987	0.46	1.24
QY_{relTDP}	$\frac{Abs_{PBS}}{Abs_{TDE/P}} \cdot \frac{Em_{TDE/P}}{Em_{PBS}}$	1.934	0.36	1.57

Table 3.4 Absorption (Abs.) and fluorescence intensities (Em.) maxima of dye solutions in PBS buffer, TDE (97%) and TDP were measured as well as the corresponding wavelengths. * [62].

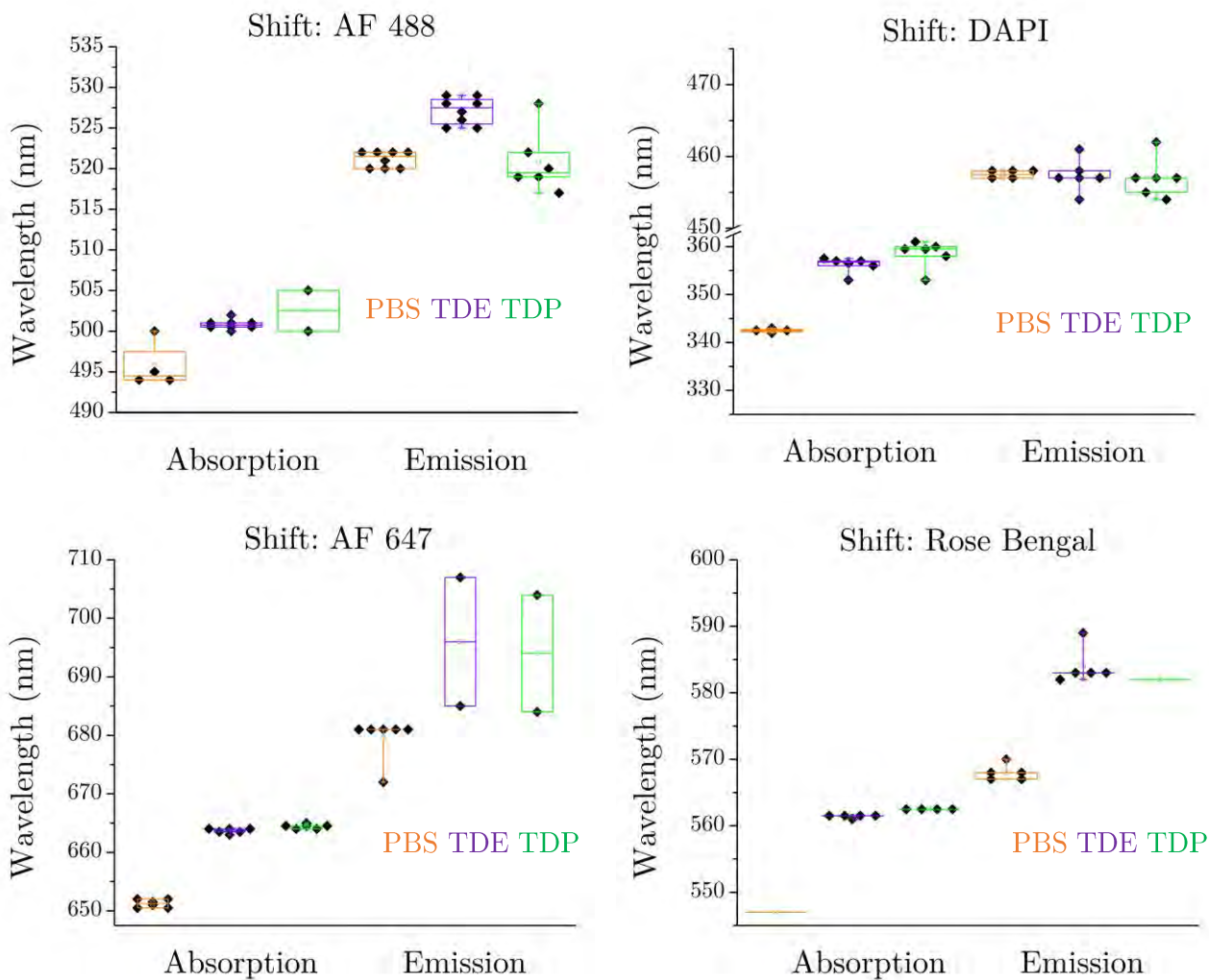


Figure 3.5. Intensity peak for absorption and emission spectra measured in three solvents PBS (orange), TDE (violet) and TDP (green). Black dots represent experimental data.

3.4 Standard staining using fluorescent phalloidins.

In order to establish a “standard” for the labeling of actin cytoskeleton with conjugated phalloidins, ProLong Diamond, a widely used mounting medium containing an antifade reagent, has been used. Figure 3.6 shows the result of the cytochemistry with HEK293 cells, the fluorescence of actin filaments is showed in red and the nucleus in blue. The bright field image shows the shape of the cells.

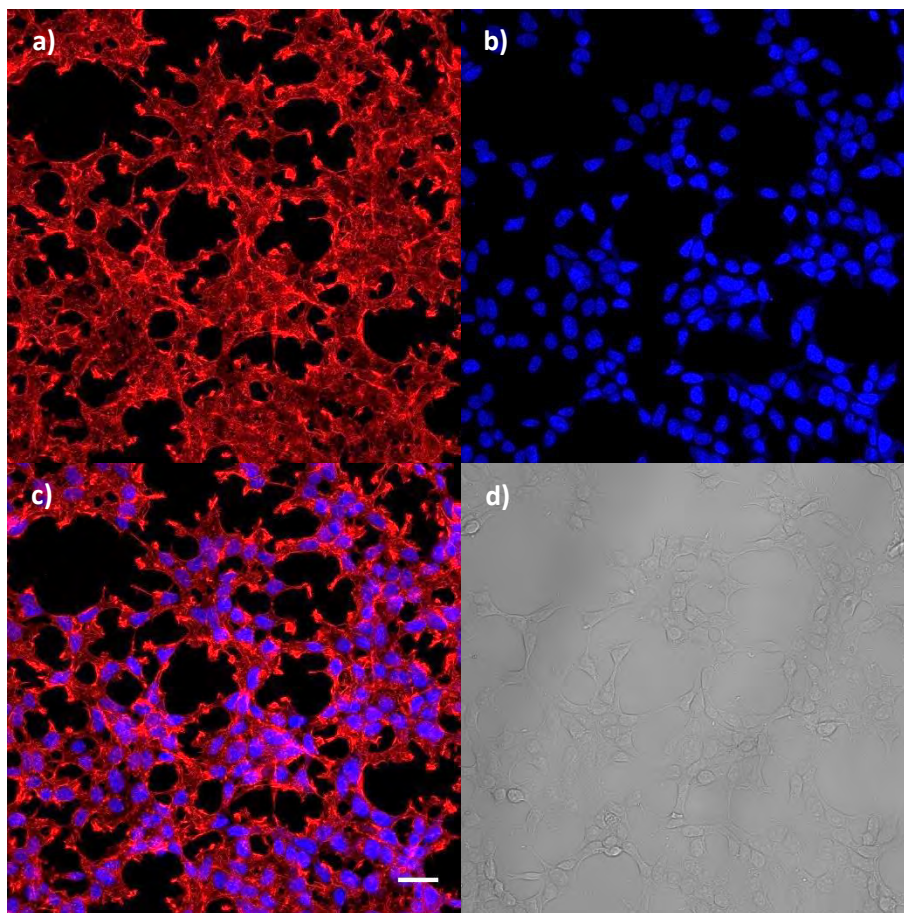


Figure 3.6 Confocal fluorescence micrographs of HEK293 cells mounted in coverslips using PLD, a) F-actin stained with Alexa Fluor 647 phalloidin, b) nuclei stained with DAPI, c) merge of both channels and d) bright field image. Micrographs were taken with a 25X objective. Scale bar: 30 μm .

The cells were then stained following the same protocol, but mounted using TDE.

The images obtained from slides prepared this way are shown in Figure 3.7

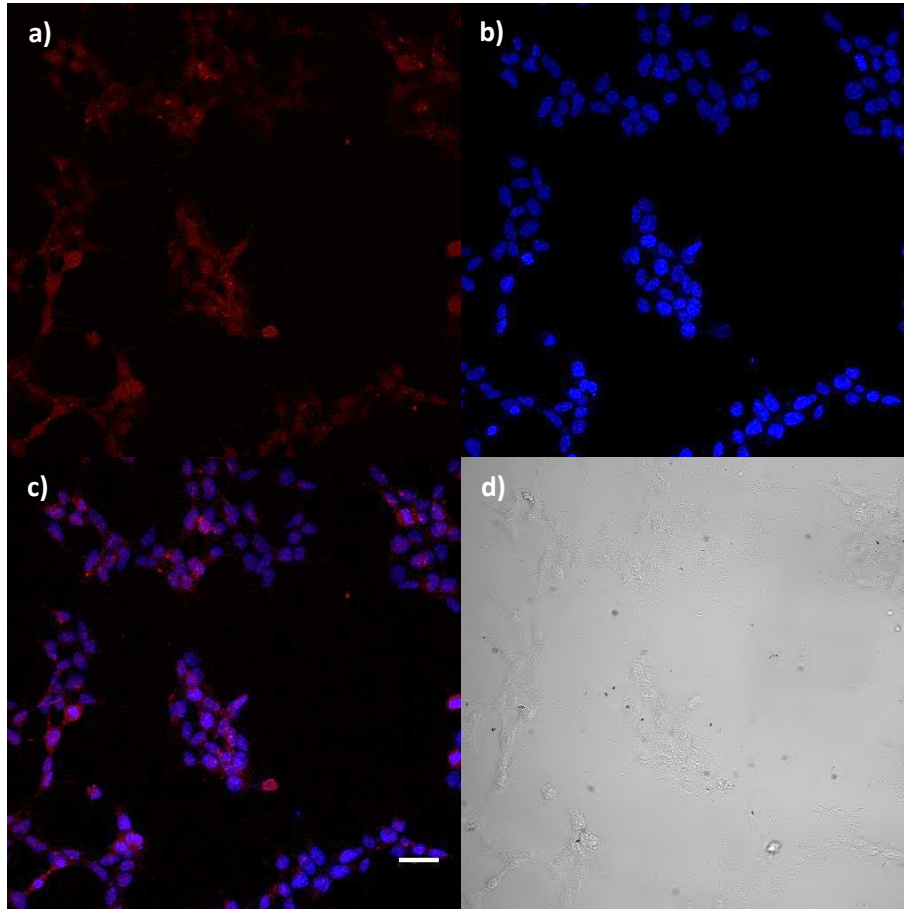


Figure 3.7. Confocal fluorescence micrographs of HEK293 cells mounted using TDE, a) Alexa Fluor 647 phalloidin-stained f-actin display reduced fluorescence and apparent altered morphology, b) nuclei stained with DAPI maintain their morphology as expected c) the merge of both channels show that the red fluorescence corresponding to the labeling with conjugated phalloidin is almost lost. d) Bright field image. The use of TDE as mounting medium reduces the contrast because refractive index of medium and glass are matched. Scale bar: $30 \mu m$.

In cells mounted with TDE, fluorescence of actin filaments looks diffuse compared to cells mounted in PLD. When using Alexa Fluor 647 phalloidin, it is visible that the distribution of red fluorescence is inespecifici in cells mounted with TDE. The structures that fluoresce in red, when using PLD are lamellipodia and the actin mesh work, seen on all the borders of the cells; on the other hand, these structures are not

distinguishable when using TDE. The DAPI staining of the nucleus is not altered by the mounting medium.

The same procedure was repeated with two different cell lines, HeLa and SH-SY5Y, which contain characteristic and distinguishable forms of actin cytoskeletons. Figure 3.8 shows the loss of localization of conjugated phalloidin when using TDE as mounting medium, in HeLa and SH-SY5Y cells. The destabilization of the fluorescent phalloidin labeling by TDE was already known, as well as its independence from the conjugated dye [37]. In this project three different dyes conjugated to phalloidin have been used: Alexa Fluor 488, 568 and 647, obtaining the same results with each one of them.

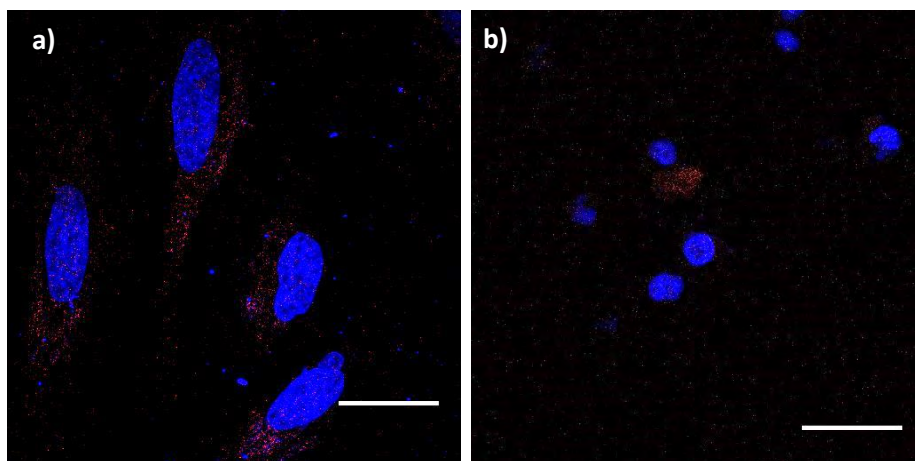


Figure 3.8 Micrographs of a) HeLa cells nuclei labeled with DAPI and F-actin labeled with Alexa Fluor 568 phalloidin. b) SH-SY5Y cells labeled with DAPI for the nucleus and Alexa Fluor 647 phalloidin for F-actin. In both a) and b), TDE was the mounting medium. It is not possible to see the actin filaments for both cell lines. Images shown are representative of 19/23 cell slides stained with phalloidin conjugated fluorophores. Images were taken using a 63X objective. Scale bar: 30 μm .

3.5 Micrographs obtained using candidates

After adjusting the pH of candidates, TDP and SDE were then used as mounting media with samples stained with conjugated phalloidins and the resulting images were compared to the micrographs obtained with the commercial medium PLD.

SDE has been used with HEK and HeLa cells labeled with conjugated phalloidins and in all the slides prepared, no fluorescence was detected for actin filaments as shown in Figure 3.9.

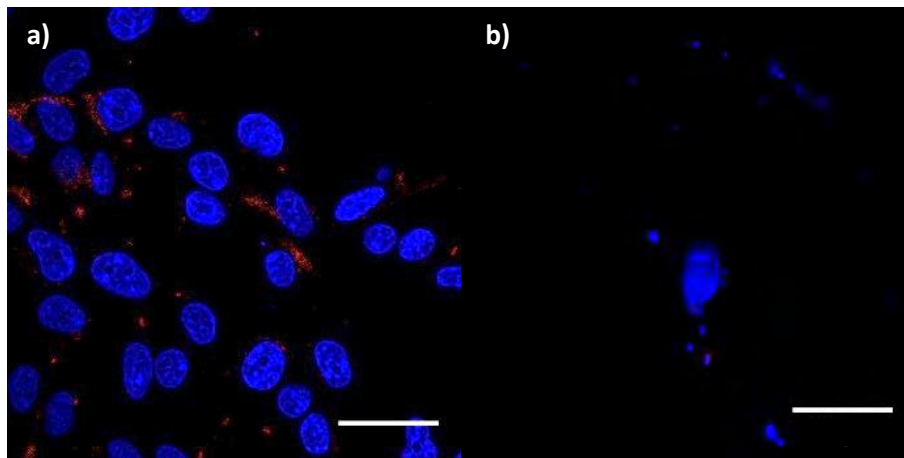


Figure 3.9 Cells mounted in SDE. Cells were stained with DAPI for the nucleus. a) HEK293 cells, stained with Alexa Fluor 647 phalloidin for F-actin, b) HeLa cells, stained with Alexa Fluor 568 phalloidin for F-actin. The fluorescence of conjugated phalloidin is not visible in any case. Three independent staining experiments were performed and 7/8 slides showed the same result.

The images obtained when using SDE do not show almost any phalloidin fluorescence at all. If compared with TDE, when using TDE there is some fluorescence but it is not specific. SDE structure differs from TDE in the two oxygens that cover the sulfur atom. With these experiments, the hypothesis that covering the sulfur atom would avoid the loss of specificity of the conjugated-phalloidin staining could be dismissed.

Cells stained with phalloidin conjugated fluorophores were mounted in coverslips using TDP as mounting medium. Images representative of multiple slides are presented in Figures 3.10-13. From 32 cell slides mounted in TDP, 23 showed actin cytoskeleton structures with the same characteristics than slides mounted in PLD. When labeled with AF 488 phalloidin, 6/6 slides showed defined actin cytoskeleton, for, AF 568 phalloidin 8/11 and for AF 647 phalloidin 9/17 present the same behavior.

3.5.1 Cytoskeleton of cells mounted in TDP

The most prominent actin structures in HeLa cells are stress fibers [63]. The actin cytoskeleton presents thick and dense stress fibers since these are the structures that are responsible for cell attachment to some substrates, as shown in Figure 3.10. The stress fibers are well conserved in both cases and no difference is observed between HeLa cells mounted in PLD and TDP. Also, the fluorescence of the probes used, DAPI and Alexa Fluor phalloidins, is comparable to the fluorescence obtained when mounting with PLD.

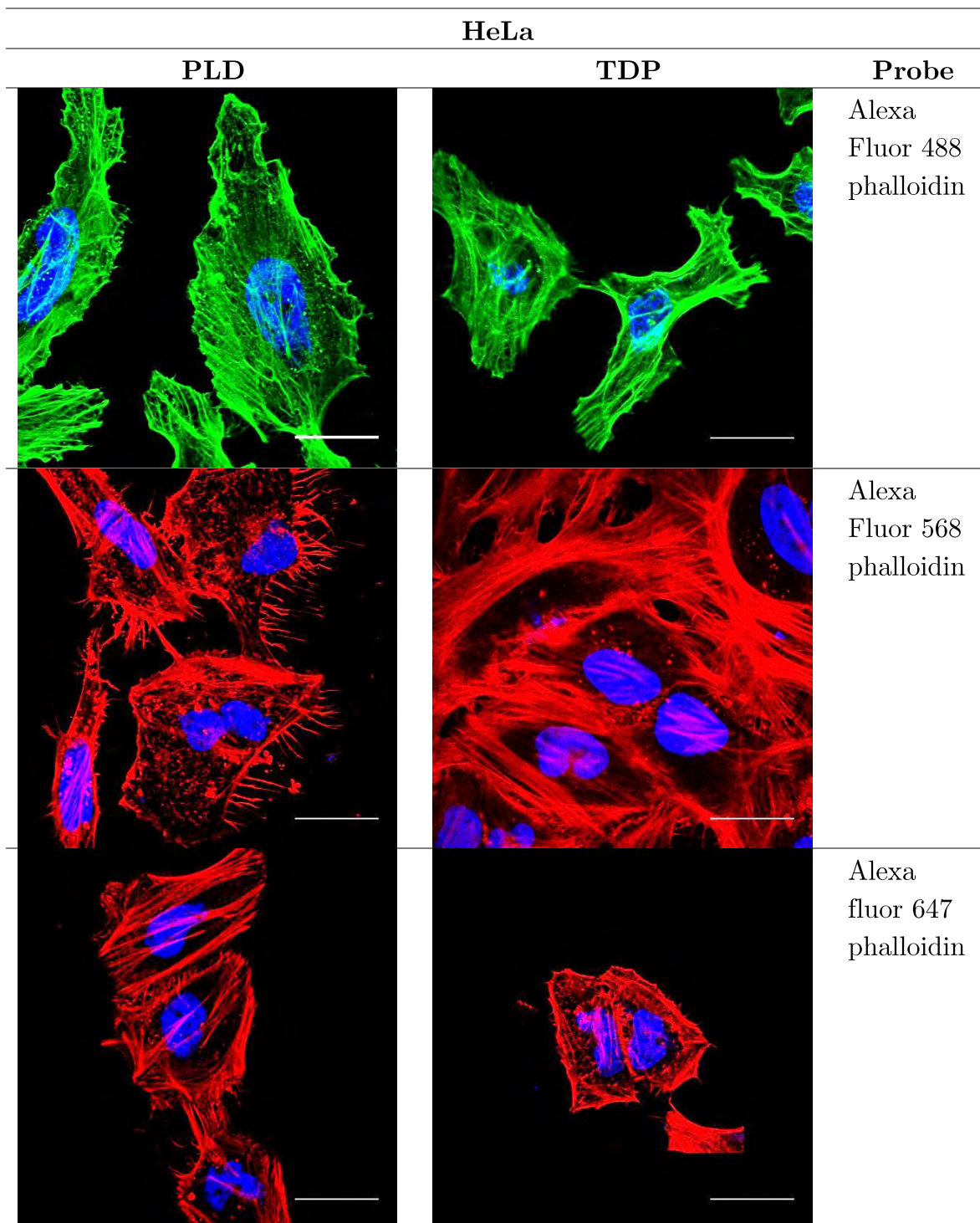


Figure 3.10 Micrographs of HeLa cells mounted in PLD and in TDP. Nuclei is stained with DAPI and f-actin with AF phalloidins. Confocal images obtained with a 63X objective. Scale bar 30 μm .

HEK 293 cells are smaller than HeLa and when cultured on glass substrates their actin cytoskeleton is visible in the form of an actin meshwork and lamellipodia. In this thesis work, HEK293 cells were labeled with Alexa Fluor 488 and 647. The micrographs obtained with TDP as mounting medium do not differ from the images obtained with PLD. Cytoskeleton of HEK 293 cells is well preserved and fluorescence of probe stays in filaments.

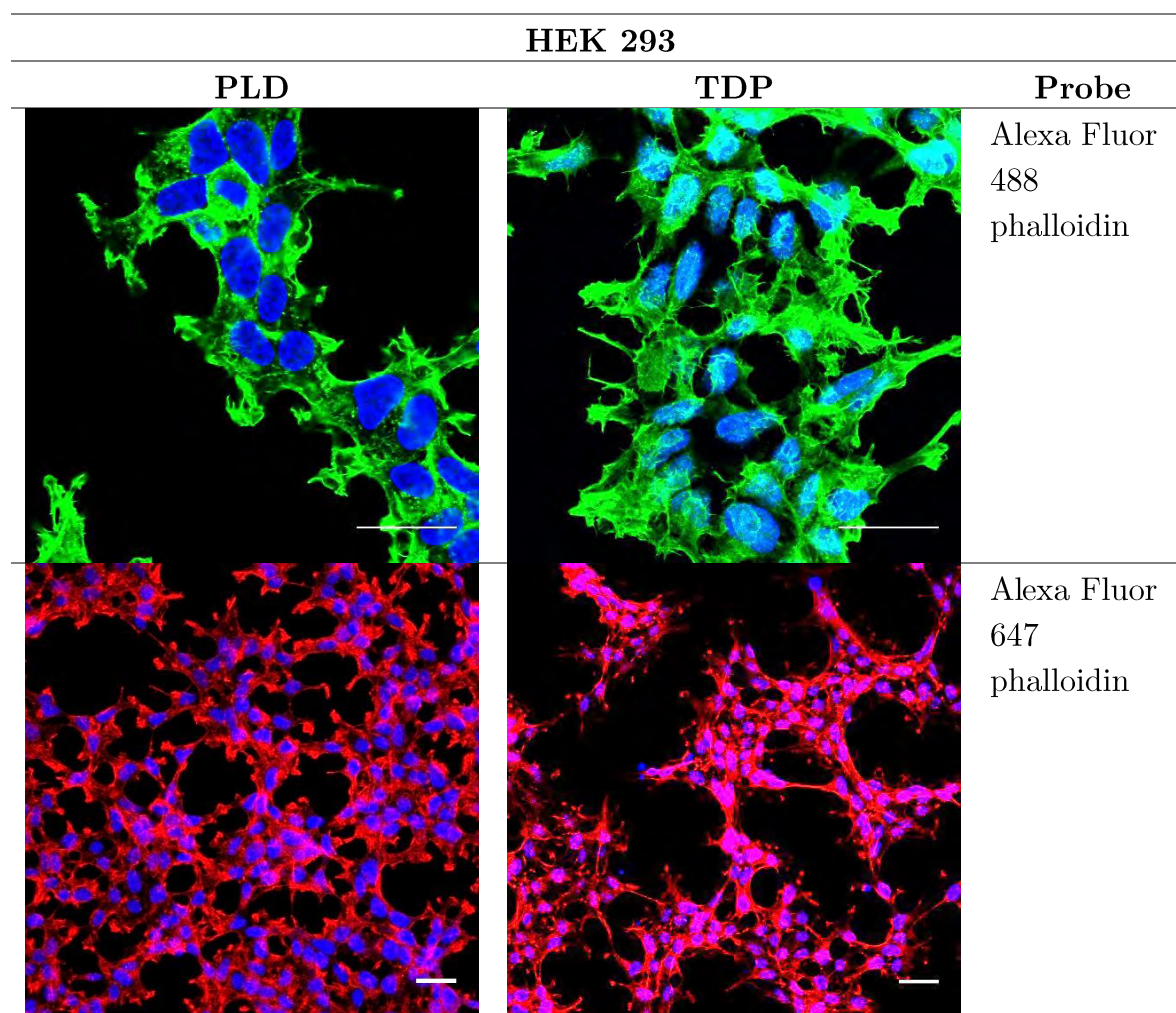


Figure 3.11. Micrographs of HEK 293 cells mounted in PLD and in TDP. Images of Hek 293 cells labeled with AF 488 were taken with a 63X objective and cells labeled with AF 647 were taken with a 25X objective. Scale bar: 30 μm .

The third cell line used is SH-SY5Y. These neuron-like cells are also smaller than HeLa (SHSY-5Y diameter is 12 μm and HeLa 20 μm [64]). SH-SY5Y are polarized

and show lamellipodia in one side which are well defined when imaging using TDP as mounting medium.

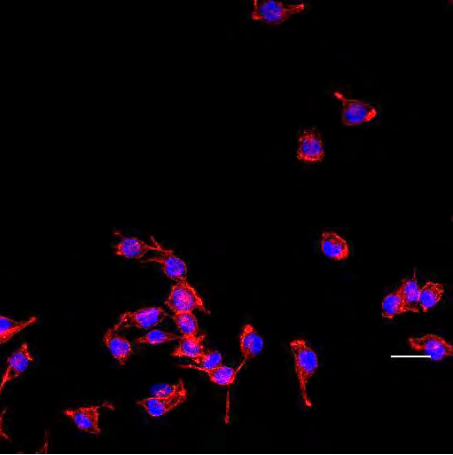
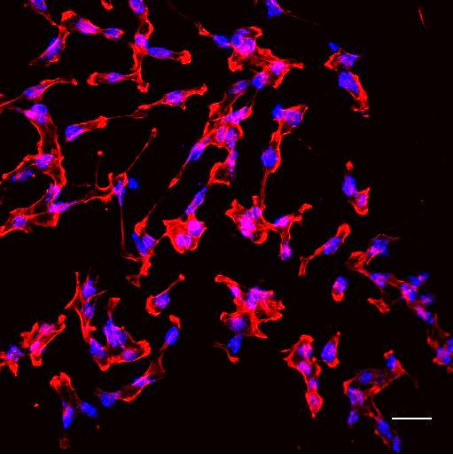
SH-SY5Y		
VECTASHIELD	TDP	Probe
		Alexa Fluor 647

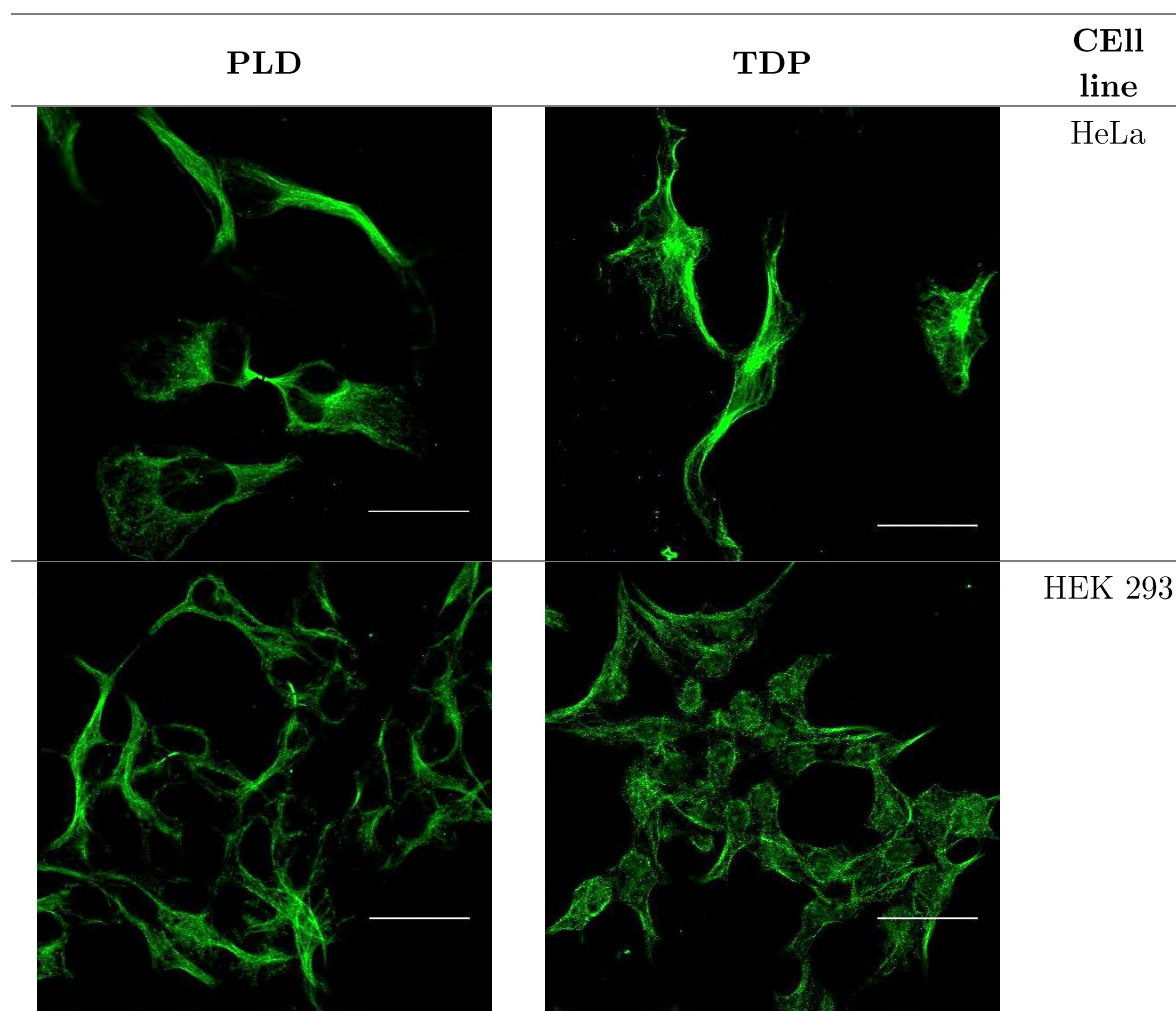
Figure 3.12 SH-SY5Y cells stained with DAPI (nucleus in blue) and actin cytoskeleton labeled with AF 647 phalloidin (red). Confocal images obtained with a 25X objective. Scale bars: 30 μm .

As shown in previous images, cell morphology when using TDP as mounting medium, was maintained with the three cell lines used. TDP did not produce shrinkage of cells, when incorporated to cells in a stepwise manner (data not shown), and no other morphological change was observed. The fluorescence of phalloidin conjugated fluorophores in presence of TDP has always been observed with Alexa Fluor 488 phalloidin (see Appendix 2), but when using the red phalloidins we experienced some variability in the outcome of the experiments. The cell slides mounted with a first batch of TDP, produced fluorescent images that maintained localized fluorescence even when re-imaged after six months. However, performing experiments with the following batches of the product gave inconclusive results. The certificate of analysis given by Sigma-Aldrich indicates that the second batch of product is less pure than the first one, 98.6% compared to 99% pure. A Raman spectroscopic characterization

of both batch has been performed, finding differences between all the batches with different experimental behavior (see Appendix 1.)

3.5.2 Microtubules of cells mounted in TDP

Immunostaining of microtubules is possible when using TDP as mounting medium. The microtubules maintain their shape and structure. Fluorescence of dye conjugated to antibody is not affected.



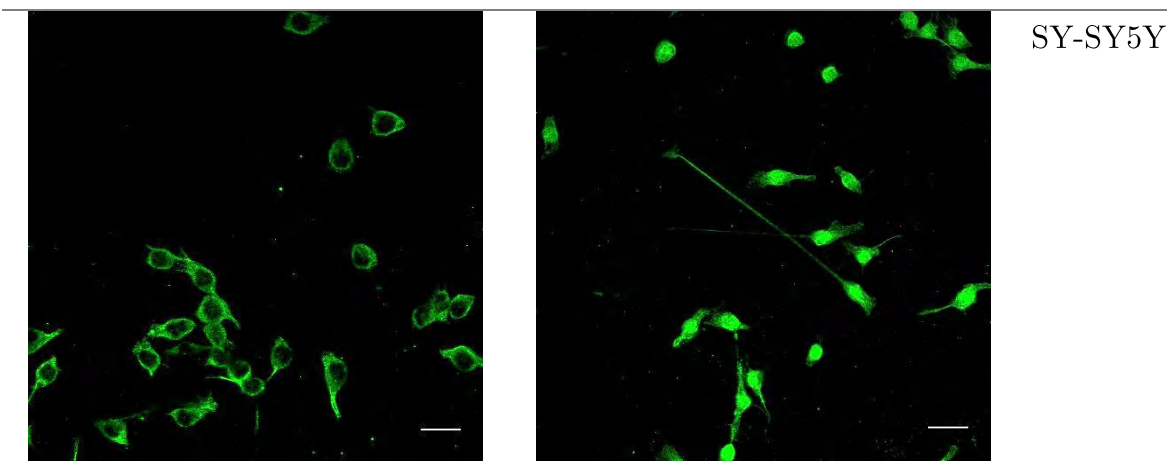


Figure 3.13. Cells with immunolabeled microtubules mounted in PLD (left) and in TDP (right). Alexa Fluor 488 is the fluorophore conjugated to antibody. Micrographs of HeLa and HEK 293 cells were obtained with a 63X objective and SH-SY5Y with a 25X objective. Scale bars: 30 μm .

3.6 Understanding loss of fluorescence of the actin filaments in presence of TDE

Explaining the reason for the loss of fluorescence associated to actin filaments with TDE mounting could provide useful chemical hints for guiding the search for improved mounting media. The first hypothesis is that fluorescence of the probes fades in presence of TDE. Through experiments, we showed that TDE does not bleach the dye, because when the same dye is conjugated to antibodies, it still fluoresces even if mounted in TDE as is shown in Figure 3.14. The second hypothesis is that TDE interacts with either phalloidin or F-actin at their binding site and then the probe, unbound from F-actin, diffuses in the medium, losing its selective binding to actin filaments. A third hypothesis cannot be excluded in principle: TDE destroys actin filaments.

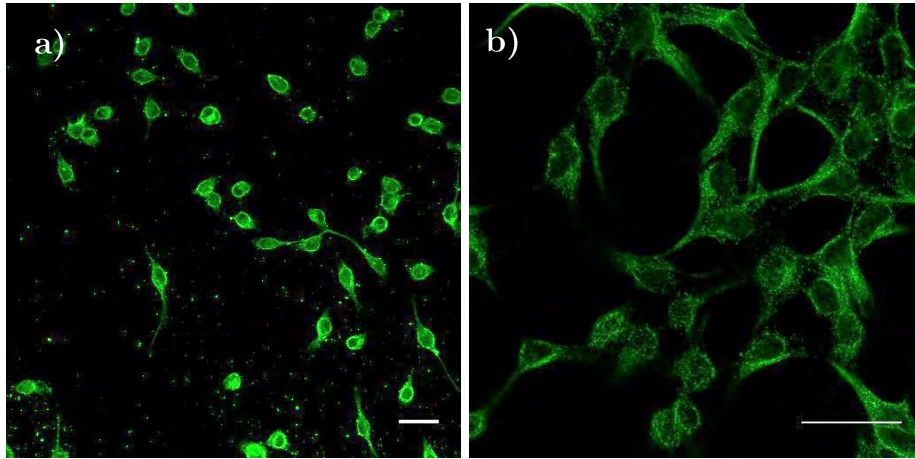


Figure 3.14 Microtubules labeled with anti-tubulin conjugated to AF 488 and mounted in TDE a) SH-SY5Y cells imaged with a 25X objective. b) HEK 293 cells imaged with a 63X objective. Scale bar 30 μm .

The microtubules that were stained with an antibody conjugated to AF 488 show fluorescence. The AF 488 is one of the fluorophores conjugated to phalloidin, that were used. When staining was performed with the fluorophore conjugated to phalloidin, the labeling did not show fluorescence.

This result implies that the fluorophore is not damaged by TDE, because the same dye conjugated to an antibody fluoresces in the usual way, but when conjugated to phalloidin it does not label the f-actin as it should.

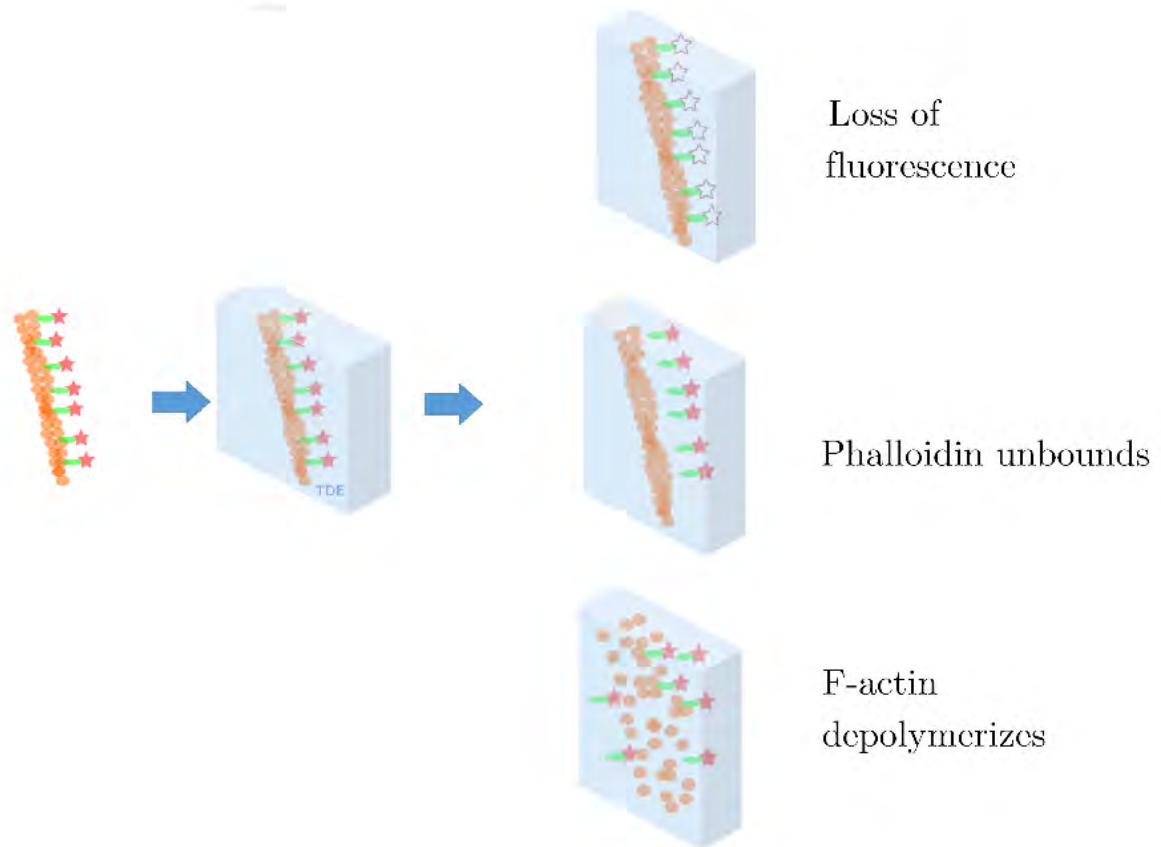


Figure 3.15 Three possible explanations for the loss of fluorescence of f-actin in presence of TDE.

First, the intensity of the emission spectra of fluorescent phalloidins dissolved in TDE has been measured 6 times along two weeks. The measurements were performed at the same wavelength on each occasion.

The normalized intensity recorded is shown in Figure 3.16. The intensity is stable in all the period of time. The sample being measured was kept on refrigeration and protected from light as is recommended for fluorophore preservation. According to this result no loss of fluorescence of conjugated phalloidins, is due to bleaching caused by TDE in time.

When cell slides mounted in TDE are imaged right after being mounted, there is still fluorescence of f-actin, as stained with phalloidins, but some minutes after the fluorescence is difusse, as is shown in Figure 3.17. As fluorophores are stable in TDE, the loss of fluorescence of cell slides could be produced because fluorophores detached from F-actin.

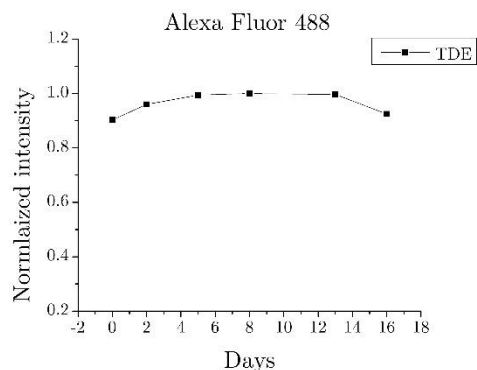


Figure 3.16 Stability of the fluorescence intensity of AF 488 measured over 16 days. The data suggest that AF 488 phalloidin’s fluorescence is maintained in time.

When cells labeled with conjugated-phalloidins are mounted in TDE a gradual loss of fluorescence is observed. In Figure 3.16, HEK 293 stained with AF 488 phalloidin are shown. Cells were imaged right after mounting (0 hr.) and every two hours at the same focal plane. After 6 hours no fluorescence was observed. The images shown here are equally adjusted in brightness and contrast, otherwise no fluorescent signal would be visible from 2 to 6 hours.

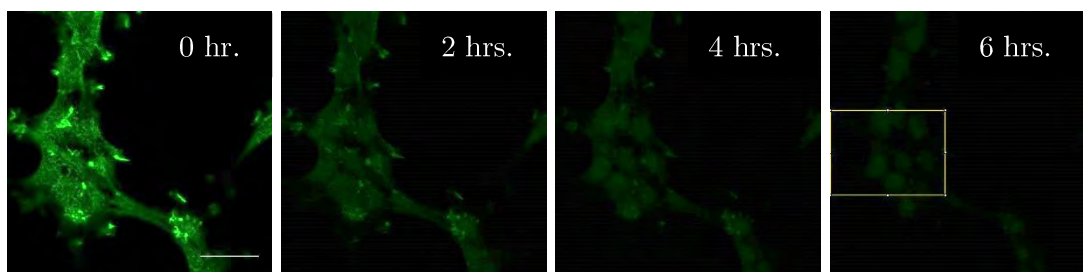


Figure 3.17 HEK 293 cells stained with AF 488 phalloidin. The rectangular section in last image (6 hrs.) corresponds to the area in which profile plot was applied.

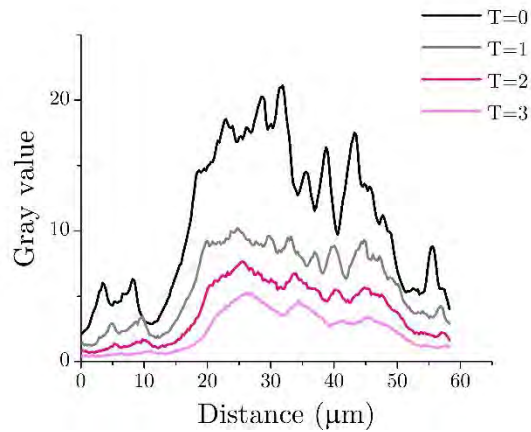


Figure 3.18 Averaged fluorescence intensity of pixels of the rectangular section in Figure 3.15. The x-axis represents the horizontal distance through the selection and the y-axis the vertically averaged pixel intensity [65].

In figure 3.18 the intensity from a rectangular section is shown. At time 0 the intensity maximum is around 20 and at time 3, after 6 hours, the maximum is around 5. The most of the intensity is lost between the first two hours.

Micrographs from Figure 3.17, apart from reduced intensity, seem to loss specificity. The more intense features at time 0 are lamellipodia and they seem to have vanished from subsequent images. As fluorescence should be maintained in time, then fluorophores should still fluoresce, but as being sparse their fluorescence in confocal system does not record anything but background.

Knowing that sparse fluorophore in media still fluoresces an experiment designed to determine if fluorophore is present in mounting media was performed. The process of mounting cell slides stained with fluorescent phalloidins was simulated with adherent cells growth in wells suitable for spectrophotometric measurements. Figure 3.19 shows the average of six measurements for emission spectra of AF 488 phalloidin. This experiment includes three different conditions for the measurement of the spectra. Black curves correspond to emission spectrum of cells stained with the probe

and then incubated with pre-mounting solutions and finally incubated for 4 hours with the mounting medium. The mounting media are PBS and TDE, then all steps of pre-mounting and mounting were performed similarly, as described in materials and methods. The pre-mounting solution was removed from cells and collected into another well and the emission spectra relative to the pre-mounting solution is shown in red. The same way the mounting medium was transferred to an empty well and measured separately, green curve.

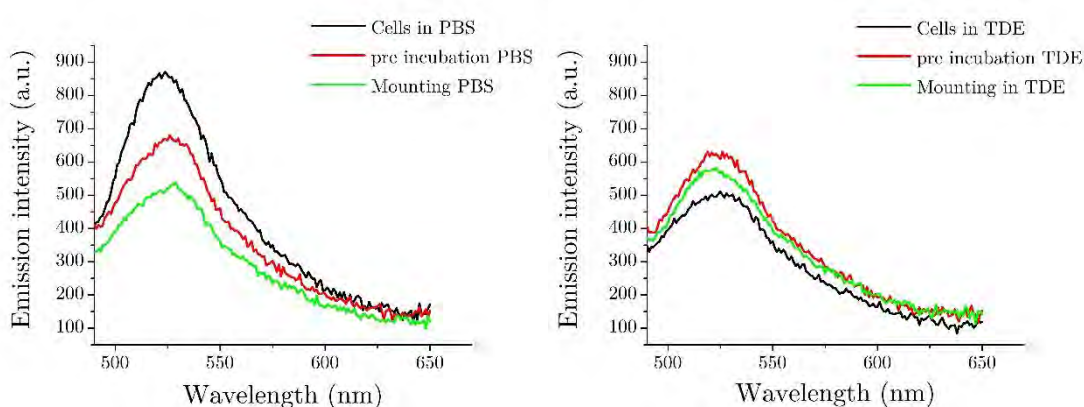


Figure 3.19 Emission spectra measured from wells containing cells stained with AF 488 phalloidin, obtained at the end of the staining procedure (black curves), wells containing pre mounting incubations media (red curves) and wells containing the media used for mounting (blue curves), in this case incubated for 4 hours.

The result of these measurements indicates that when using PBS, most of the fluorescence remains in the wells containing cells, suggesting that the cell-fluorophore interaction is stable, even if some fluorophores are lost from cells and diffuse into the media. The emission spectra for the solutions used in the experiment performed with TDE suggest that fluorescence stays mostly in the pre-mounting solution, while the wells containing cells are the least fluorescent. It should be noted that AF 488

phalloidin's intensity is reduced when using TDE as solvent, thus the intensity recorded for TDE might correspond to a higher amount of fluorophore.

An additional hypothesis considers that TDE could be able to destabilize the actin cytoskeleton in fixed cells, therefore destroying microfilaments before conjugated phalloidin could bind to them. Figure 3.20 shows the result of a preliminary experiment designed to verify if actin filaments were still present after incubation with TDE. Actin filaments were not visible in cells that were incubated in TDE and then extensively rinsed.

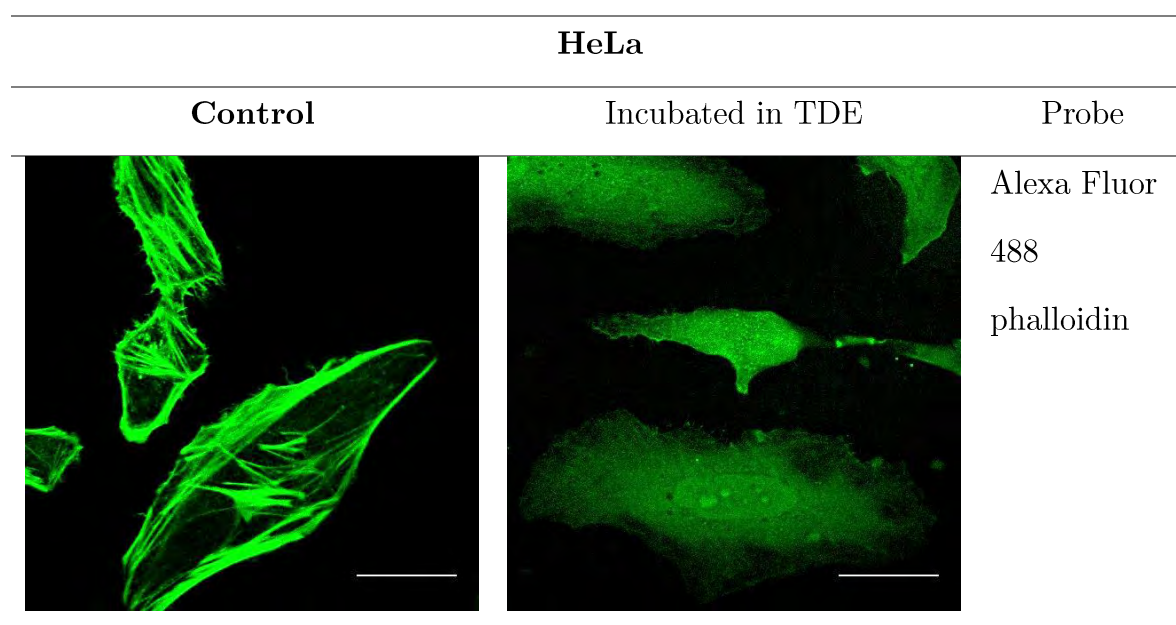


Figure 3.20 Actin cytoskeleton organization of HeLa cells labeled with AF488 phalloidin. a) Control cells, b) cells labeled with fluorescent phalloidin after incubation in TDE and several washing steps to remove TDE from cells. Cells were mounted using PLD as mounting medium.

This result seem to suggest that actin filaments are depolymerized in presence of TDE. However, due to the fact that cellular proteins are very stable after aldehyde fixation and that no chemical is known to selectively destroy only one cellular component after fixation, we hypothesize that the apparent lack of localized actin

fluorescent could be due mostly to incomplete removal of the viscous TDE from cellular spaces, which could then hinder the binding of phalloidin. A definitive proof for these hypotheses could only be obtained by transmission electron microscopy of unstained cells, after TDE incubation.

3.7 Molecular dynamics

The results shown here are the initial part of a work that intends to simulate a system composed by F-actin, phalloidin and TDE. Using molecular dynamics will allow us to understand the effect of solvating with TDE, F-actin labeled with phalloidin. MD simulations approach will help us to determine if there is an interaction between TDE and phalloidin or TDE and actin filaments.

With the MD simulations we will obtain the mean residence time and contact distance between TDE-phalloidin and TDE-F-actin. According to these information and comparing with the same parameters reported for F-actin-phalloidin [66] we will be able to determine if the possible interaction interferes with the labeling of F-actin.

The simulation of the system composed by F-actin, phalloidin and solvated with TDE requires the use of a supercomputer, because of the high number of atoms involved (>100 000). In order to perform the simulation in a reasonable time, computational infrastructure was obtained from the supercomputer of the Laboratorio Nacional del Sureste (LNS), located at Puebla, Mexico.

First of all, spatial distribution of atoms and force fields for TDE, phalloidin and F-actin was obtained. A protein data bank (PDB) is commonly used to obtain position of atoms, which were previously acquired from X-ray or NMR. The primary

information stored in the PDB file consists of a list of the atoms for each protein and their location in space.

For F-actin, PDB file used is 2ZWH [67] optimized for CHARMM force field, previously used by [66]. Also, TDE and phalloidin are described using same force field. In case of TDE and phalloidin, PDB files were obtained from SwissParam website [68], which provides topology and parameters for small organic molecules compatible with the CHARMM all atoms force field. SwissParam site needs a MOL2 file in order to render the PDB, thus MOL2 was obtained from ZINC website, which is a database for commercially-available compounds [69].


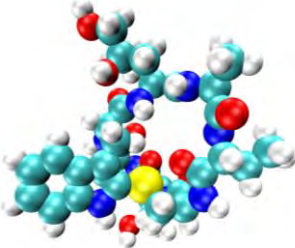
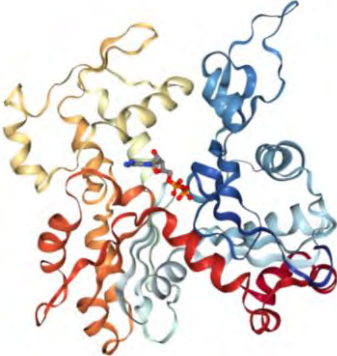
	Atomistic model	Number of atoms
TDE		17
Phalloidin		103
Actin monomer		2961

Table 3.5 Atomic representation of TDE, phalloidin and an actin monomer.

As a first step TDE's force field used to describe intermolecular interaction, was used to reproduce thermodynamic properties. Energy minimization was performed using 1 000 molecules of TDE at 400 K in a canonical ensemble (NVT) until the thermodynamic equilibrium was reached. Then an annealing process was simulated in an isobaric-isothermal (NPT) ensemble at 1 atm. Temperature was decreased by $\Delta T = 50 K$ until 300 K was reached. In this case the mean value of TDE's density given by the simulation is 1107 Kg/m^3 as shown in Figure 3.21, and the value reported in literature is 1179.5 Kg/m^3 [43].

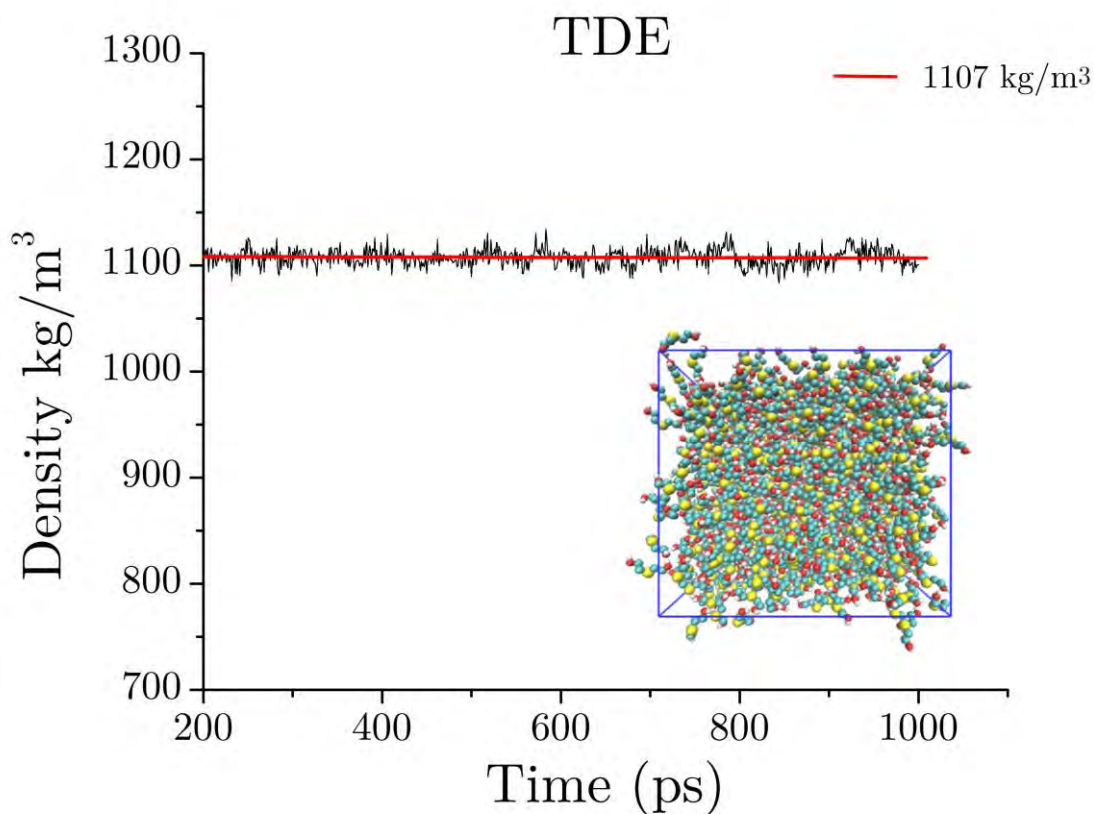


Figure 3.21 TDE's density obtained from simulation. Cubic box of filled with 1000 TDE molecules.

In the second simulation the TDE-phalloidin system has been studied. The system was previously equilibrated for 1 ns in a canonical ensemble (NVT) using Berensen thermostat. An annealing process was required to decrease temperature of the system. The annealing process was performed in an NPT ensemble. Temperature was reduced by $\Delta T = 50 K$. Length of simulation for each temperature was 1 ns, and final temperature 300 K. The box contains 200 molecules of TDE and 10 phalloidins. The mean value for density is 1190 Kg/m^3 , compared to density for pure TDE, the system TDE-phalloidin has a higher density as expected. It was observed during simulation that phalloidin aggregates.

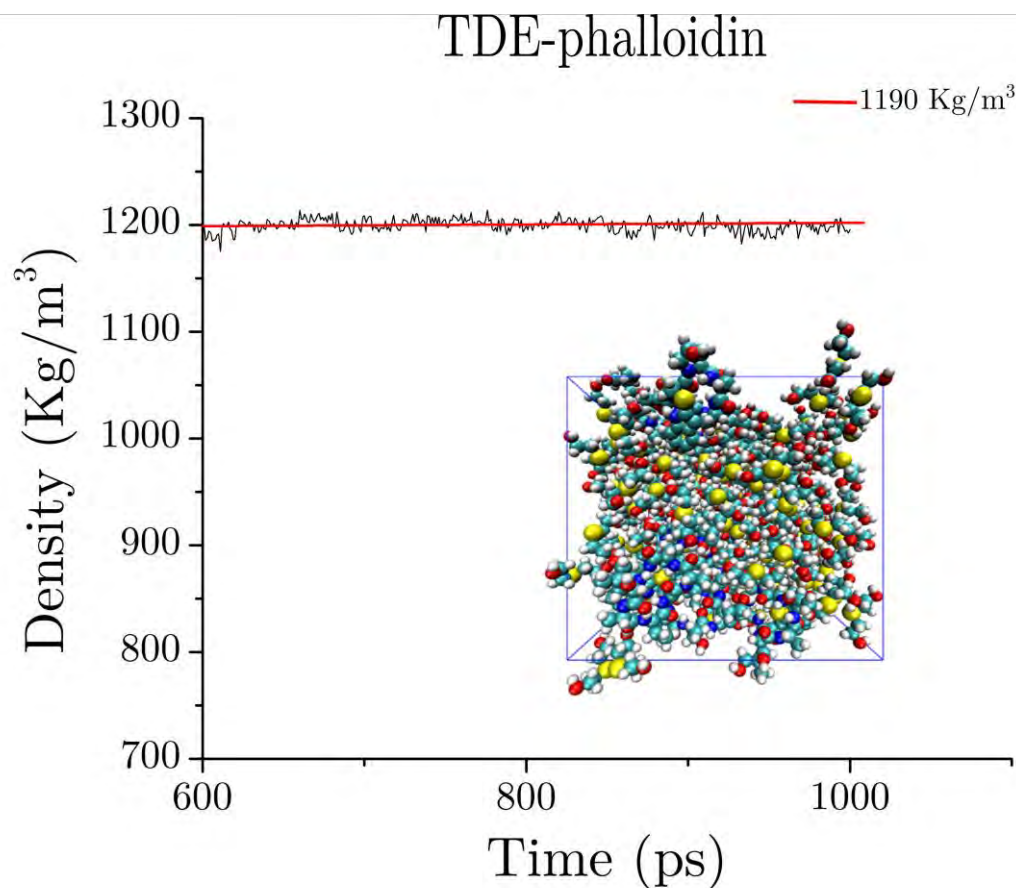


Figure 3.22 Density of the system TDE-phalloidin. 200 molecules of TDE and 10 molecules of phalloidin.

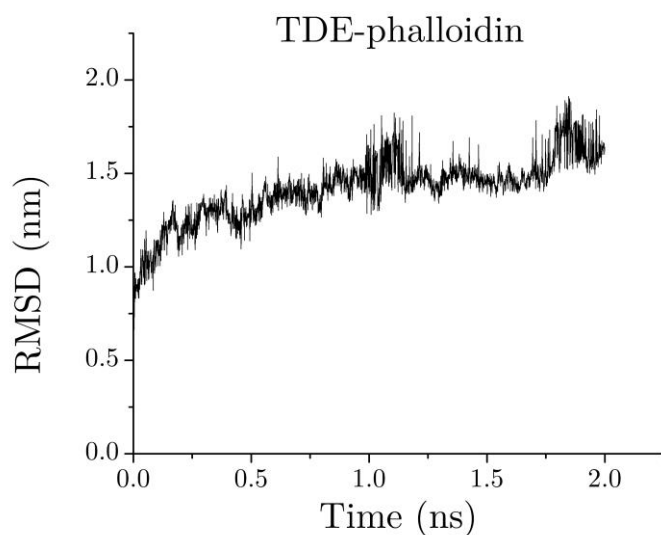


Figure 3.23 Root mean square deviation of TDE atoms with respect to phalloidin.

The values of RMSD obtained for TDE respect to phalloidin are increase in time, showing that TDE distance from phalloidin increases respect to initial situation.

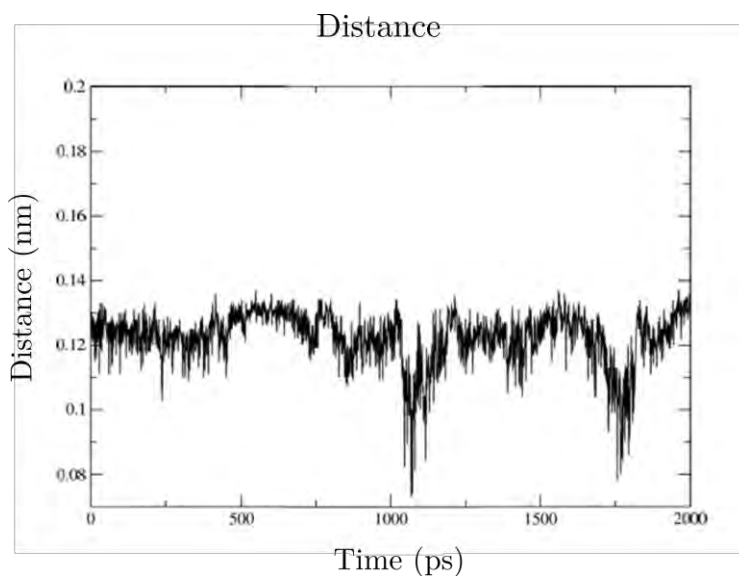


Figure 3.24 Contact distance of TDE from phalloidin.

As is shown in Figure 3.24 minimal contact distance between a TDE molecule and phalloidin is around 0.12 nm. From Figure 3.23 and 3.24 we can interpret that even when there are TDE molecules close to phalloidin all the time at a distance that is

quite constant (0.12 nm) these molecules are not the same that were close to phalloidin when the simulation started. The RMSD indicates that distance of TDE molecules with respect to an initial phalloidin increases in a period of 2 ns.

One of the hypothesis for the loss of fluorescence in actin filaments is that dye unbinds from filaments, this could be possible because of interaction between TDE and phalloidin or TDE and F-actin. When phalloidin was solvated with TDE no interaction was observed.

Another step, to be performed in a future work, is the simulation that includes actin monomers and phalloidin. The idea is that by means of contact distance and residence time determine if simulation shows an affinity between actin monomers and phalloidin. It is known that phalloidin has affinity for F-actin and not for monomers. Figure 3.25 shows the cubic box containing actin monomers and phalloidin.

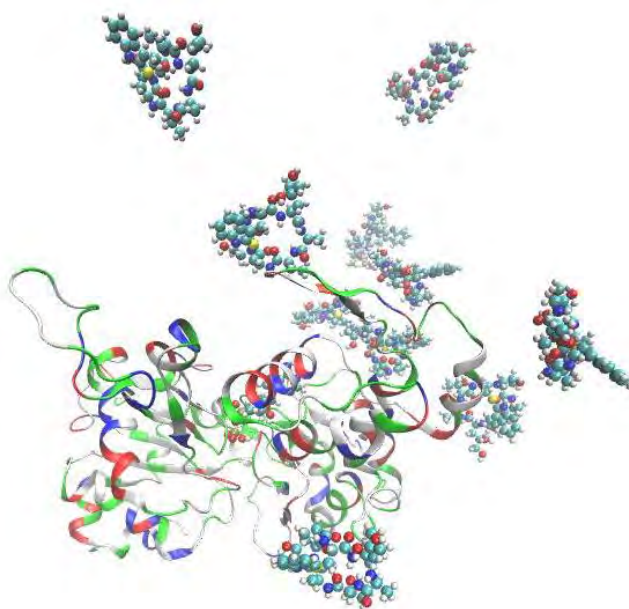


Figure 3.25 Phalloidin in ribbon diagram and phalloidin in atomistic representation.

It is important to mention that to form one actin filament 13 monomers are usually included [67], then the system of interest composed by F-actin, TDE and phalloidin, will be formed by more than 100 000 atoms. Time needed to simulate this kind of system by a supercomputer and for no more than 10 ns, is about 1 month. The simulation of the whole system is a task that is left for a further work.

Conclusion and further work

The focus of this work is to propose the use of 3,3'-thiodipropanol as mounting medium compatible with cytochemistry of actin cytoskeleton of fixed cells. The most used method for labeling F-actin in fixed cells, phalloidin conjugated fluorophores were used in this work. Three dyes conjugated to phalloidin were tested, showing that TDP preserves the fluorescence of phalloidin conjugated fluorophores in actin filaments. The staining and imaging was tested in three cell lines.

In this work, the probes tested with TDP are AF488 Anti-tubulin, DAPI, AF 488 phalloidin, AF 568 phalloidin, AF 647 phalloidin. When mounted in TDP, performance of all of those probes was successful. The only exception is AF 647 that has showed good performance only whit TDP the first purchased lot that had a purity of 99%, but the results were difficult to replicate with the second purchased lot of TDP (purity= 98.6%). The Raman spectra of these two different lots indicate that there are impurities in the second TDP that are not present in the first one. Analysis of these spectra could provide information about the loss of fluorescence of actin filaments when labeled with conjugated phalloidins. Comparison between components present on TDP of lot 2 and TDE might give suggestions about the chemical agents that affect the staining.

As future works, TDP need to be tested with cell slides stained with other fluorescent probes. The solvatochromism and relative quantum efficiency of the probes should also be reported.

Compared to TDE, TDP has some advantages and also disadvantages. Refractive index of TDP is not as high as the one of TDE, although is much higher than the refractive index of many commercial media, but the possibility of performing staining with fluorescent phalloidins certainly represents an interesting difference.

The mixture of TDE and TDP also needs to be characterized: the features of chemical mixtures are not always the expected ones, so it could happen that the characteristics of one medium prevail on those of the other medium. Current experiments are defining if TDE/TDP mixtures could have high refractive index and be conjugated-phalloidins compatible.

Also, experiments are under the way in which different light sources are used to obtain the dispersion curve of TDE and TDP in the whole visible spectra.

References

- [1] J. Hogg, *The Microscope: Its History, Construction, and Applications*. Illustrated London Libr., 1834.
2. Greenberg, G. L. *The light microscope: Its use and development* By W.G. Hartley Senecio Publishing Co., Oxford (1993) ISBN 0-906831-05-9
- [3] Pawley, *Handbook of Biological Confocal Microscopy*. Springer Science & Business Media, 2010.
- [4] S. Hell, G. Reiner, C. Cremer, and E. H. K. Stelzer, “Aberrations in confocal fluorescence microscopy induced by mismatches in refractive index,” *J. Microsc.*, vol. 169, no. 3, pp. 391–405, Mar. 1993.
- [5] T. D. Visser, J. L. Oud, and G. J. Brakenhoff, “Refractive index and axial distance measurements in 3-D microscopy,” *Optik*, vol. 90, no. 1, pp. 17–19, 1992.
- [6] P. Török, P. Varga, Z. Laczik, and G. R. Booker, “Electromagnetic diffraction of light focused through a planar interface between materials of mismatched refractive indices: an integral representation,” *JOSA A*, vol. 12, no. 2, pp. 325–332, Feb. 1995.
- [7] K. Carlsson, “The influence of specimen refractive index, detector signal integration, and non-uniform scan speed on the imaging properties in confocal microscopy,” *J. Microsc.*, vol. 163, no. 2, pp. 167–178, Aug. 1991.
- [8] I. Escobar, G. Saavedra, M. Martínez-Corral, and J. Lancis, “Reduction of the spherical aberration effect in high-numerical-aperture optical scanning instruments,” *JOSA A*, vol. 23, no. 12, pp. 3150–3155, Dec. 2006.
9. Wiley: *Fluorescence Microscopy: From Principles to Biological Applications*, 2nd Edition - Ulrich Kubitscheck.
- [10] E. Abbe, “Beiträge zur Theorie des Mikroskops und der mikroskopischen Wahrnehmung.”
- [11] L. R. S. R. S., “XV. On the theory of optical images, with special reference to the microscope,” *Lond. Edinb. Dublin Philos. Mag. J. Sci.*, vol. 42, no. 255, pp. 167–195, Aug. 1896.
- [12] A. Egner and S. W. Hell, “Fluorescence microscopy with super-resolved optical sections,” *Trends Cell Biol.*, vol. 15, no. 4, pp. 207–215, Apr. 2005.
- [13] W. Ockenga, “Optical Contrast Methods,” *Leica Sci.*, Jun. 2011.
- [14] F. Zernike, “How I discovered phase contrast,” *Science*, vol. 121, no. 3141, pp. 345–349, Mar. 1955.
- [15] L. Schermelleh, R. Heintzmann, and H. Leonhardt, “A guide to super-resolution fluorescence microscopy,” *J. Cell Biol.*, vol. 190, no. 2, pp. 165–175, Jul. 2010.
- [16] M. J. Sanderson, I. Smith, I. Parker, and M. D. Bootman, “Fluorescence Microscopy,” *Cold Spring Harb. Protoc.*, vol. 2014, no. 10, p. pdb.top071795, Oct. 2014.
- [17] P. Mazzarello, “A unifying concept: the history of cell theory,” *Nat. Cell Biol.*, vol. 1, no. 1, pp. E13–E15, May 1999.
18. Scherer, W. F., Syverton, J. T. & Gey, G. O. Studies on the propagation in vitro of Poliomyelitis viruses. *J. Exp. Med.* 97, 695–710 (1953).
- [19] H. Eagle, “Nutrition Needs of Mammalian Cells in Tissue Culture,” *Science*, vol. 122, no. 3168, pp. 501–504, 1955.

- [20] O. Shimomura, F. H. Johnson, and Y. Saiga, "Extraction, purification and properties of aequorin, a bioluminescent protein from the luminous hydromedusan, *Aequorea*," *J. Cell. Comp. Physiol.*, vol. 59, pp. 223–239, Jun. 1962.
- [21] P. R. Yadav, *Cell Culture*. Discovery Publishing House, 2008.
- [22] F. L. Graham, J. Smiley, W. C. Russell, and R. Nairn, "Characteristics of a human cell line transformed by DNA from human adenovirus type 5," *J. Gen. Virol.*, vol. 36, no. 1, pp. 59–74, Jul. 1977.
- [23] J. L. Biedler, L. Helson, and B. A. Spengler, "Morphology and growth, tumorigenicity, and cytogenetics of human neuroblastoma cells in continuous culture," *Cancer Res.*, vol. 33, no. 11, pp. 2643–2652, Nov. 1973.
- [24] "ATCC: The Global Bioresource Center." [Online]. Available: <https://www.atcc.org/>. [Accessed: 20-Oct-2017].
- [25] D. Leyton-Puig, K. M. Kedziora, T. Isogai, B. van den Broek, K. Jalink, and M. Innocenti, "PFA fixation enables artifact-free super-resolution imaging of the actin cytoskeleton and associated proteins," *Biol. Open*, vol. 5, no. 7, pp. 1001–1009, Jul. 2016.
- [26] F. Capani, T. J. Deerinck, M. H. Ellisman, E. Bushong, M. Bobik, and M. E. Martone, "Phalloidin-eosin followed by photo-oxidation: a novel method for localizing F-actin at the light and electron microscopic levels," *J. Histochem. Cytochem. Off. J. Histochem. Soc.*, vol. 49, no. 11, pp. 1351–1361, Nov. 2001.
- [27] M. C. Jamur and C. Oliver, "Permeabilization of cell membranes," *Methods Mol. Biol. Clifton NJ*, vol. 588, pp. 63–66, 2010.
28. Wiley: Current Protocols Select: Methods and Applications in Microscopy and Imaging - Simon Watkins, Claudette St. Croix.
- [29] B. Alberts, A. Johnson, J. Lewis, M. Raff, K. Roberts, and P. Walter, "Looking at the Structure of Cells in the Microscope," 2002.
- [30] N. Panchuk-Voloshina *et al.*, "Alexa dyes, a series of new fluorescent dyes that yield exceptionally bright, photostable conjugates," *J. Histochem. Cytochem. Off. J. Histochem. Soc.*, vol. 47, no. 9, pp. 1179–1188, Sep. 1999.
31. Immunological Properties of an Antibody Containing a Fluorescent Group. Experimental Biology and Medicine - Albert H. Coons, Hugh J. Creech, R. Norman Jones, 1941.
- [32] S. Ravikumar, R. Surekha, and R. Thavarajah, "Mounting media: An overview," *J. Dr NTR Univ. Health Sci.*, vol. 3, no. 5, p. 1, Mar. 2014.
- [33] "MilliporeSigma | United States," *Sigma-Aldrich*. [Online]. Available: <http://www.sigmaaldrich.com/united-states.html>. [Accessed: 20-Oct-2017].
34. Biomeda gel/mount aqueous, <http://carefordescientific.com/electron-biomeda-gel-mount-aqueous-17985-10-100496-546-biomeda-gel-mount-aqueous-20ml-each-20ml/>. (Accessed: 20th October 2017)
- [35] "Vector Laboratories: State of the Art Labeling and Detection | Vector Labs." [Online]. Available: <https://vectorlabs.com/>. [Accessed: 20-Oct-2017].
- [36] "Thermo Fisher Scientific." [Online]. Available: <https://www.thermofisher.com/mx/es/home.html>. [Accessed: 20-Oct-2017].
- [37] T. Staudt, M. C. Lang, R. Medda, J. Engelhardt, and S. W. Hell, "2,2'-thiodiethanol: a new water soluble mounting medium for high resolution optical microscopy," *Microsc. Res. Tech.*, vol. 70, no. 1, pp. 1–9, Jan. 2007.

- [38] M. G. Gustafsson, D. A. Agard, and J. W. Sedat, "15M: 3D widefield light microscopy with better than 100 nm axial resolution," *J. Microsc.*, vol. 195, no. Pt 1, pp. 10–16, Jul. 1999.
- [39] C. Fouquet *et al.*, "Improving axial resolution in confocal microscopy with new high refractive index mounting media," *PloS One*, vol. 10, no. 3, p. e0121096, 2015.
- [40] S. Bretschneider, C. Eggeling, and S. W. Hell, "Breaking the diffraction barrier in fluorescence microscopy by optical shelving," *Phys. Rev. Lett.*, vol. 98, no. 21, p. 218103, May 2007.
- [41] M. Ono, T. Murakami, A. Kudo, M. Isshiki, H. Sawada, and A. Segawa, "Quantitative comparison of anti-fading mounting media for confocal laser scanning microscopy," *J. Histochem. Cytochem. Off. J. Histochem. Soc.*, vol. 49, no. 3, pp. 305–312, Mar. 2001.
- [42] W. Zhu, Y. Knapp, and V. Deplano, "Low hazard refractive index and density-matched fluid for quantitative imaging of concentrated suspensions of particles," *Exp. Fluids*, vol. 57, no. 5, p. 68, May 2016.
43. CRC Handbook of Chemistry and Physics, 84th Edition Edited by David R. Lide (National Institute of Standards and Technology). CRC Press LLC: Boca Raton. 2003. ISBN 0-8493-0484-9. J. Am. Chem. Soc. 126, 1586–1586 (2004).
- [44] "The PubChem Project." [Online]. Available: <https://pubchem.ncbi.nlm.nih.gov/>. [Accessed: 28-Nov-2017].
- [45] N. A. Campbell and J. B. Reece, *Biology, 6th Edition*, 6th edition. San Francisco: Benjamin Cummings, 2001.
- [46] G. M. Cooper, "Structure and Organization of Actin Filaments," 2000.
- [47] T. Wieland, "The toxic peptides from Amanita mushrooms," *Int. J. Pept. Protein Res.*, vol. 22, no. 3, pp. 257–276, Sep. 1983.
- [48] E. M. De La Cruz and T. D. Pollard, "Transient kinetic analysis of rhodamine phalloidin binding to actin filaments," *Biochemistry (Mosc.)*, vol. 33, no. 48, pp. 14387–14392, Dec. 1994.
49. Thermo Fisher Scientific. Available at: <https://www.thermofisher.com/search/supportSearch?type=Chemical+Structures&query=12379>. (Accessed: 28th November 2017)
- [50] G. Lukinavičius *et al.*, "Fluorogenic probes for live-cell imaging of the cytoskeleton," *Nat. Methods*, vol. 11, no. 7, pp. 731–733, Jul. 2014.
- [51] J. Riedl *et al.*, "Lifeact: a versatile marker to visualize F-actin," *Nat. Methods*, vol. 5, no. 7, p. 605, Jul. 2008.
- [52] A. Hospital, J. R. Goñi, M. Orozco, and J. L. Gelpí, "Molecular dynamics simulations: advances and applications," *Adv. Appl. Bioinforma. Chem. AABC*, vol. 8, pp. 37–47, Nov. 2015.
- [53] M. P. Allen, "Introduction of Molecular Dynamics Simulation," *Comput. Soft Matter Synth. Polym. Proteins Lect. Notes Norbert Attig Kurt Bind. Helmut Grubmuller Kurt Kremer Eds NIC Ser.*, vol. vol 23, Jan. 2004.
- [54] E. Lindahl, B. Hess, and D. van der Spoel, "GROMACS 3.0: a package for molecular simulation and trajectory analysis," *Mol. Model. Annu.*, vol. 7, no. 8, pp. 306–317, Aug. 2001.
- [55] "Knowledge Base of Mini-Chrom Monochromators | Dynasil." [Online]. Available: <https://www.dynasil.com/product-category/mini-chrom-monochromators/>. [Accessed: 28-Nov-2017].

- [56] J. Rheims, J. Köser, and T. Wriedt, “Refractive-index measurements in the near-IR using an Abbe refractometer,” *Meas. Sci. Technol.*, vol. 8, no. 6, p. 601, 1997.
- [57] “Spectral characteristics of Molecular Probes actin-selective probes—Table 11.2.” [Online]. Available: <https://www.thermofisher.com/mx/es/home/references/molecular-probes-the-handbook/tables/spectral-characteristics-of-our-f-actin-selective-probes.html>. [Accessed: 28-Nov-2017].
- [58] A. Diaspro, F. Federici, and M. Robello, “Influence of refractive-index mismatch in high-resolution three-dimensional confocal microscopy,” *Appl. Opt.*, vol. 41, no. 4, pp. 685–690, Feb. 2002.
- [59] “ChemicalBook---Chemical Search Engine.” [Online]. Available: <http://www.chemicalbook.com/>. [Accessed: 28-Nov-2017].
- [60] A. Samoc, “Dispersion of refractive properties of solvents: Chloroform, toluene, benzene, and carbon disulfide in ultraviolet, visible, and near-infrared,” *J. Appl. Phys.*, vol. 94, no. 9, pp. 6167–6174, Oct. 2003.
- [61] S. Kedenburg, M. Vieweg, T. Gissibl, and H. Giessen, “Linear refractive index and absorption measurements of nonlinear optical liquids in the visible and near-infrared spectral region,” *Opt. Mater. Express*, vol. 2, no. 11, pp. 1588–1611, Nov. 2012.
- [62] “Life Technologies.” [Online]. Available: <https://www.thermofisher.com/mx/es/home.html>. [Accessed: 28-Nov-2017].
- [63] P. Maupin and T. D. Pollard, “Improved preservation and staining of HeLa cell actin filaments, clathrin-coated membranes, and other cytoplasmic structures by tannic acid-glutaraldehyde-saponin fixation,” *J. Cell Biol.*, vol. 96, no. 1, pp. 51–62, Jan. 1983.
- [64] “Search BioNumbers - The Database of Useful Biological Numbers.” [Online]. Available: <http://bionumbers.hms.harvard.edu/search.aspx?log=y&task=searchbytrmorg&trm=sh+sy+5y&time=2017%2f11%2f29+11%3a51%3a49.366>. [Accessed: 29-Nov-2017].
- [65] J. Schindelin *et al.*, “Fiji: an open-source platform for biological-image analysis,” *Nat. Methods*, vol. 9, no. 7, pp. 676–682, Jul. 2012.
- [66] J. Pfaendtner, E. Lyman, T. D. Pollard, and G. A. Voth, “Structure and dynamics of the actin filament,” *J. Mol. Biol.*, vol. 396, no. 2, pp. 252–263, Feb. 2010.
- [67] T. Oda, M. Iwasa, T. Aihara, Y. Maéda, and A. Narita, “The nature of the globular- to fibrous-actin transition,” *Nature*, vol. 457, no. 7228, pp. 441–445, Jan. 2009.
- [68] V. Zoete, M. A. Cuendet, A. Grosdidier, and O. Michielin, “SwissParam: A fast force field generation tool for small organic molecules,” *J. Comput. Chem.*, vol. 32, no. 11, pp. 2359–2368, Aug. 2011.
- [69] J. J. Irwin, T. Sterling, M. M. Mysinger, E. S. Bolstad, and R. G. Coleman, “ZINC: A Free Tool to Discover Chemistry for Biology,” *J. Chem. Inf. Model.*, vol. 52, no. 7, pp. 1757–1768, Jul. 2012.

Appendix 1

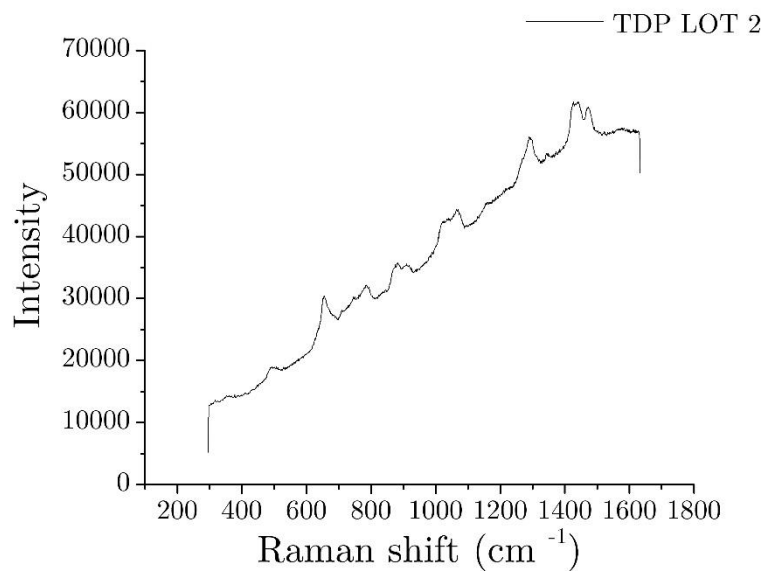
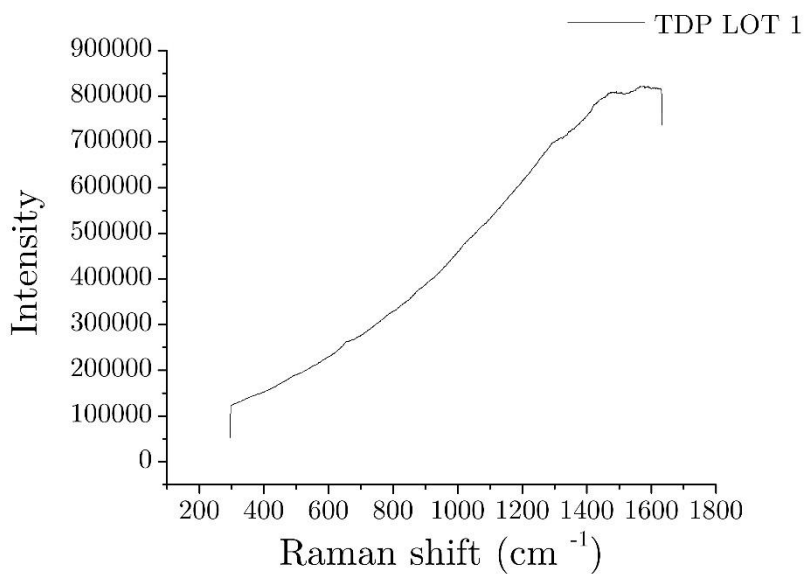


Figure A.1 Raman spectrum of TDP. Spectra of lot 2 presents peaks in the region from 300 to 1600, when laser wavelength used is 514. Lot 1 does not present these peaks.

Appendix 2

Statistics of micrographs

TDE

Number slides imaged	f-actin defined	F-actin not defined	Ratio of f-actin defined	Ratio of f-actin no defined	% defined	% not defined
23	2	21	2/23	21/23	8.7%	91.3%

TDP

Number slides imaged	F-actin defined	F-actin not defined	Ratio of f-actin defined	Ratio of f-actin no defined	% defined	% not defined
34	23	11	23/34	11/34	67.6%	32.4%

	Number slides imaged	F-actin defined	F-actin not defined	Ratio of f-actin defined	Ratio of f-actin no defined	% defined	% not defined
AF 488	6	6		6/6	0	100%	0%
AF 568	11	8	3	8/11	3/11	72.7%	23.3%
AF 647	17	9	8	9/17	8/17	52.9%	47.1
LOT 1	4	4	0	4/4	0	100%	0%
LOT 2	13	5	8	5/13	8/13	38.5%	61.5%

SDE

Number cell slides imaged	F-actin defined	F-actin not defined	Ratio of f-actin defined	Ratio of f-actin no defined	% defined	% not defined
9	1	8	1/8	7/8	12.5%	87.5%